PEOPLE'S DEMOCRATIC REPUBLIC OF ALGERIA

Ministry of Higher Education and Scientific Research

University of Amar Telidji - Laghouat

Faculty of Sciences

Department of Materials Science

MASTER THESIS

DOMAINE : Materials Science

Discipline : Physics

OPTION : Materials physics

BENMILOUD Rokaya

Theme

Structural, Electronic, Magnetic and Mechanical Properties of Mn-based AntiPerovskites

Jury members :

KHENCHOUL Salah	MCA	President
CHERIET Abderrahmane	MCB	Examiner
LAGOUN Brahim	MCA	Supervisor
KORIBA Imane	PhD student	Co-supervisor

2020 / 2021

Dedication

In the memory of my dear father.

I hope my DAD has a front row seat in heaven

to watch me graduate!

I Love you and I MISS you

Acknowledgements

First and foremost, I am grateful to Allah almighty who granted me the power and the patience to finish my work and to finally reach my goal.

Then I would like to express my deepest gratitude to my supervisor Dr. Brahim LAGOUN for believing in me through my darkest time and his unaccountable guidance, support, patience and for teaching me so much insightful knowledge in my travel through the world of material physics. He has been a great source of inspiration that guided me toward the end of this work.

A warm Salutation goes to my Co-supervisor PhD student. Imane KORIBA for her constant support, and for her valuable comments and feedback. This work would not have been accomplished without her effort and instructions.

I thank profusely all the members of the jury in this case Dr. KHENCHOUL Salah and Dr. CHERIET Abderrahmane *for agreeing to judge this humble work.*

I am particularly grateful to the director of the material physicochemistry laboratory of the university of Laghouat Mr.TAOUTI Mohamed also of course my sincere gratitude to the laboratory members for being a wonderful community in which to 'grow up' as a research student, the personal and professional relationships forged in this year will stay with me forever.

I am lucky and richly blessed to have you my dear friends, especially Aicha, Nada, Aroua, and Namarek.

Finally, saying this with pride, love and sincere heart the memories and the face of each teacher, doctor and professor in the material sciences department will forever be with me and a great part of my life's journey.

My deepest appreciation belongs to my father's soul especially then all my family who always kept me going and fighting, this work would not have been possible without them.

To my FAMILY,

From the moment I came to this life you have been around loving me and careing for me, you've always been my backup and support, thanks to you I'm what I am today, I would never reach what I have accomplished, my personality, my science degree,... all i have is thanks to you.

To MAMA for her advice, her patience, and her faith, because she always understood.

To Zohra my only sister I just don't know what I would have done without you.

In writing this thesis, I have drowned so many times, I awe a particular debt to my brother Mohamed for leading and helping me.

To Ahmed i just want to let you know you mean the world to me, only a heart as dear as yours would give so unselfishly.

I don't believe in superheroes from fantasy cause i live with one, and that's you, Ali I love you ♡.

To my brothers's wifes the many things you' ve done, all the times that you care, even though i might not say i appreciate all you do, I feel blessed having you.

To our children I love you for always being my tiny best friends and a blessing to me.

Table of Contents

List of tables

List of figures

“Optimism is the one quality more associated with success and happiness than any other.”

-Brian Tracy

General introduction

General introduction

Magnetism is one of the oldest phenomena in the history of natural science. It is said that magnetism was first discovered by a shepherd who noticed that the iron tip of his stick was attracted by a stone. This stone was found in Asia Minor, in the Magnesia district of Macedonia or in the city of Magnesia in Ionia. The word 'magnetism' is believed to originate from these names [1].

Studies of transition metals are complicated by the fact that partially filled d bands can induce important magnetic properties. As a result, a much more subtle treatment of electron spin interactions. Presently magnetic materials constitute one of the most several research fields and show very wide variety of physical phenomena and properties [2].

Of all the metallic elements, the occurrence of magnetism only in the 3d transition metals specially (Fe, Co, Ni and Mn), and in heavy rare-earth metals such as Gd, Tb, Dy, …etc. The 3d transition metals have high Curie points and exhibit ferromagnetism with large spontaneous magnetizations at room temperature [3], so that alloys containing these metals are used as magnetic materials in a wide range of practical applications [4]. The carriers of the magnetism, the 3d electrons, are located relatively far from the atomic core, and considered as they are moving among the atoms (or itinerant), rather than localized at individual atoms [5].

In the last few years, perovskite materials proved to be one of the most important ternary systems, which attracted tremendous research interest worldwide owing to their potential applications in the present technologies and in industries [6]. The unique versatility of such perovskite crystal structure finds novel functionalities in material science and enormous potential for novel device applications [7]. In addition, a number of materials which are better described as alloys, of formula B_3AX, where A and B are metals and X is an anion or semimetal. These are often said to adopt the so-called antiperovskite or inverse perovskite structure. The B_3AX antiperovskite structure is beset by structural variations that depend upon exact composition as well as temperature and pressure, all of which have a profound significance for physical properties [8].

More specifically Mn-based APVs carbides and nitrides with the general composition Mn_3AX, are one of the most commonly explored materials in recent years, due to their novel physical properties, which have made them of potential use in several applications including superconductivity [9-10], nontrivial topological nature [11], large magnetoresistance (GMR) [12], magnetostriction [13-14], negative thermal expansion [15], and piezo magnetism [16-17].

For instance, $MgCNi_3$ is a well-known superconductor with a critical temperature of 8 K, which is unique as being the first oxygen-free superconductor with a crystal structure like perovskites [18].

One of the most challenging and interesting issue in materials research and development is predicting the crystal structure of an unknown material from first principles. The density functional theory (DFT) has proven to be one of the most accurate methods for the computation of the electronic structure and other physical properties of solids, therefore we have different methods in order to understand the physical properties: empirical methods, semi-empirical methods, and first principles methods. These first principles are known as majority calculations ab initio in the theory of functional density which specifies that the knowledge of the electron density makes it possible to determine the properties of the ground state.

In this work, we study the structural, electronic, magnetic, and mechanical properties of Mn-based antiperovskites using the theory of the functional density (DFT) and the linearized augmented plane wave method at total potential (FP-LAPW) implemented in the Wien2k code and pseudo potential-plan waves (PP-PW) implemented in the ABINIT code and we compare these properties with other works.

This memoire is organized as follows:

Firstly, in chapter 1 some definitions and notations of perovskites and antiperovskites materials are outlined. The aim here is to introduce the models used for the study of the bulk of the materials investigated during this memoire.

Chapter 2 is divided in two principal sections. In the first section we outline the basic foundations of the ground-state density functional theory. We introduce the Hohenberg- Kohn theorems and the Kohn-Sham equations and finally we describe superficially the main approximations for the exchange-correlation functional. In the second section we highlight in detail the main computational method FP-LAWP and DFPT used in our simulations.

Chapter 3 is divided in three parts: at first, presents the results of a systematic study by means of the full potential linearized augmented planewave (FP-LAPW) method of Mn-based antiperovskites and discuss the trends in their structural, electronic, and magnetic properties. Secondly, we have studied the effect of pressure in the magnetic moments. Finally, shows the results of calculations by DFPT method for Mn-based antiperovskites. I close my memoire, with a general conclusion and some perspectives.

References

[1] Chikazumi, Soshin, and Chad D. Graham. *Physics of Ferromagnetism 2e*. No. 94. Oxford University Press on Demand, 2009

[2] Ashcroft, Neil W., and N. David Mermin. "Solid state physics." *Brooks Cole* (1976).

[3] Cyrot, M., et al. "Magnetism of the rare earth, 3d–Theoretical review." *Le Journal de Physique Colloques* 40.C5 (1979): C5-171.

[4] McHenry, Michael E., and David E. Laughlin. "Magnetic properties of metals and alloys." *Physical Metallurgy*. Elsevier, 2014. 1881-2008

[5] Broddefalk, Arvid. *Magnetic properties of transition metal compounds and superlattices*. Diss. Acta Universitatis Upsaliensis, 2000.

[6] Di Giacomo, Francesco, et al. "Progress, challenges and perspectives in flexible perovskite solar cells." *Energy & Environmental Science* 9.10 (2016): 3007-3035.

[7] Varma, PC Reshmi. "Low-dimensional perovskites." *Perovskite Photovoltaics*. Academic Press, 2018. 197-229.

[8] Wang, Yonggang, et al. "Antiperovskites with exceptional functionalities." *Advanced Materials* 32.7 (2020): 1905007.

[9] He, Bing, et al. "CuNNi3: a new nitride superconductor with antiperovskite structure." *Superconductor Science and Technology* 26.12 (2013): 125015.

[10] Shein, Igor Rolenovich, Alexander Leonidovich Ivanovskii, and Nadezhda Ivanovna Medvedeva. "Electronic structure of the new MgCNi 3 superconductor and related intermetallic compounds." *Journal of Experimental and Theoretical Physics Letters* 74.2 (2001): 122-127.

[11] Yu, Rui, et al. "Topological node-line semimetal and Dirac semimetal state in antiperovskite Cu 3 PdN." *Physical review letters* 115.3 (2015): 036807.

[12] Kamishima, K., et al. "Giant magnetoresistance in the intermetallic compound Mn 3 GaC." *Physical Review B* 63.2 (2000): 024426.

[13] Shibayama, T., and K. Takenaka. "Giant magnetostriction in antiperovskite Mn3CuN." *Journal of applied physics* 109.7 (2011): 07A928.

[14] Shimizu, T., et al. "Giant magnetostriction in tetragonally distorted antiperovskite manganese nitrides." *Journal of Applied Physics* 111.7 (2012): 07A903.

[15] Hamada, T., and K. Takenaka. "Giant negative thermal expansion in antiperovskite manganese nitrides." *Journal of Applied Physics* 109.7 (2011): 07E309.

[16] Zemen, J., Z. Gercsi, and K. G. Sandeman. "Piezomagnetism as a counterpart of the magnetovolume effect in magnetically frustrated Mn-based antiperovskite nitrides." *Physical Review B* 96.2 (2017): 024451.

[17] Boldrin, David, et al. "Giant piezomagnetism in Mn3NiN." *ACS applied materials & interfaces* 10.22 (2018): 18863-18868.

[18] He, T., et al. "Superconductivity in the non-oxide perovskite MgCNi 3." *Nature* 411.6833 (2001): 54-56.

“What you get by achieving your goals is not as important as what you become by achieving your goals.”

-Henry Thoreau

Chapter I: Literature notes about Perovskites

Chapter I: Literature notes about perovskites

I.1. Introduction

As you know, throughout human history, most developments were accompanied by discovering new materials, for example semiconductor, superconductor, magnetic materials…etc.

In the recent years, perovskites, which belong to a new class of materials, have attracted attention because some of them are considered as magnetic materials that have high potential applications. For instance, the science of magnetism has an important place in today's life. So, among their main fields of use, we can mention machine tools, transport (magnetic levitation train), watchmaking (quartz watch), computer hard disks, magnetic cards, electronic banking with credit cards…etc. One of the most common applications of magnetism are medical imaging technique: magnetic resonance imaging and perhaps the most popular application to the public.

(Figure I.1) illustrate some applications of new materials:

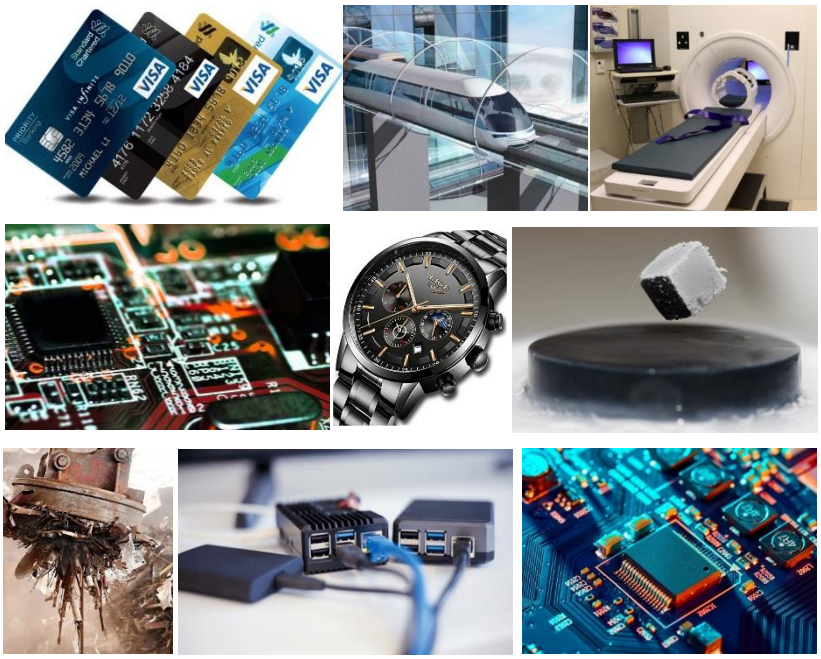

Figure I. 1: Applications of some materials [1-5].

Perovskites have been used in various technologies such as magnetic random-access-memories (RAM), colossal magnetoresistance (CMR), photocatalytic materials, magnetic refrigeration (MR) technology, electrical field sensors [6].

Chapter I: Literature notes about perovskites

I.2. Generalities about perovskites and antiperovskites materials

In 1839, in the Ural Mountains, the geologist Gustav Rose discovered the mineral $CaTiO_3$ and he named perovskite in honour of the eminent Russian mineralogist, Count Lev Alexevich von Perovski. They are usually dark brown to black, due to impurities, but when pure are clear with a refractive index of approximately 2.38.

Figure I. 2: Perovskite mineral $CaTiO_3$ [7-8].

Currently the name perovskite is used to refer to any member of ternary materials that has the formula ABX_3 where A is usually a large cation, (rare earths, alkaline earths or alkali metals) such as K, Na, Li; Sr, Ba, or Ca, and B is usually a medium-sized cation is a transition metal ion such as Ti, Ni, Fe, Co, or Mn, and X is more often a simple anion such as oxygen, halogen and hydrogen. In fact a perovskite structure mineral, Bridgmanite $(Fe,Mg)SiO_3$, is the most abundant solid phase in the earth's interior, making up 38% of the total.

The importance of perovskites became apparent with the discovery of the valuable dielectric and ferroelectric properties of barium titanate $BaTiO_3$, in the 1940s. This material was rapidly employed in electronics in the form of capacitors and transducers [9-10].

Perovskites are of different types, like simple perovskites (perovskite oxides, fluoroperovskites…) [11-12], antiperovskites (inverse perovskites) [13-14], double perovskites [15], Complex perovskites [16], and organic–inorganic hybrid perovskites [17], according to composition and chemical interaction of the constituent elements within the compound.

I.2.1. Description of crystal structure of PVs and APVs materials:

The most popular structure in perovskite materials is cubic with space group (Pm-3m n°221). The structure, illustrated in figure I.3 is simple cubic with five atoms per unit cell. The A cations occupy the corners of the cube and are surrounded by 12 anions in a cube octahedral coordination. The B cations occupy the centres of the cubes and are surrounded by 6 anions in an octahedral coordination. The anions X occupy the centre of each face of the cubes.

We can also obtain the same network by a repetition of cubic structure where the cations A occupy the centre of the cube, cations B the vertices and anions X the midpoint of edges of the cube (figure I.3).

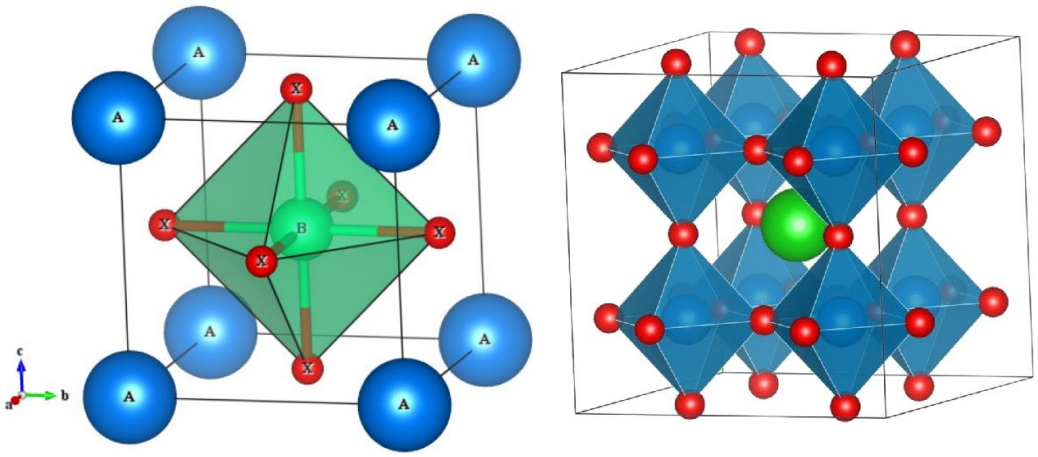

Figure I. 3: Crystallography structure of perovskites materials [18].

We find perovskites materials in different structures for example (Tetragonal-Rhombohedral-Orthorhombic...etc), (Table I.1) shows some examples of perovskites's structures.

Table I. 1: Examples of types of perovskites in different structures.

Structure	Example
Tetragonal	BaTiO3
Rhombohedral	LaNiO3
Orthorhombic	GdFeO3
Monoclinic	BiScO3
Triclinic	AgCuF3
Cubic	$LaAlO_3$
Hexagonal	$BaMnO_3$

A structure identical to the perovskite structure is also found in some materials and alloys of B_3AX compositions are called Antiperovskites (or inverse-perovskites), where A is from a wide range of metals including Al, Ga, In, Zn, Ge, Sn, Cu and others, X is either N or C, and B is a

metal, typically Mn, Cr, Fe, Ni, Ca, Ln. The structure of most known phases is cubic, space group (Pm-3m, n°221), with a lattice parameter of approximately 0.4 nm.

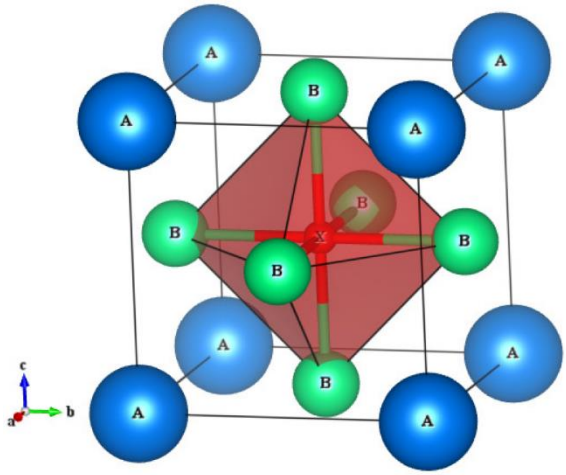

Figure I. 4: Crystallography structure of antiperovskites materials.

In this structure, the metal atom B occupies the anion position of the ideal perovskite structure, while the X atoms occupy the XB_6 octahedral positions, and the A atoms occupy the vertices of the cube. This situation arises if the B and A cations are relatively similar in size and the X anion is sufficiently small.

Many of antiperovskites are cubic or nearly cubic, but they often undergo one or more structural phase transitions, particularly at low temperatures. (Table I.2) shows some examples of antiperovskites in different structures.

Table I. 2: Examples of types of antiperovskites materials in different structures.

Structure	**Example**
Tetragonal	$GeNFe_3$
Rhombohedral	-
Orthorhombic	Ba_3PN
Monoclinic	-
Triclinic	-
Cubic	Cu_3PdN
Hexagonal	Ba_3BiP

Chapter I: Literature notes about perovskites

The number of antiperovskite compounds is still very limited compared with the great possibilities shown in the elemental periodic table. Studies on antiperovskites are still rare, with no more than fifty papers published annually, due to the relatively few quantitatively discovered antiperovskites. The concept “anti” is not widely acknowledged, and sometimes, the newly discovered antiperovskites are simply treated as intermetallic compounds or dual-metal nitrides/carbides, unaware of their unique structure. Nevertheless, the importance of antiperovskites is far beyond our expectations. Usually, monovalent, or divalent cations are located at the X site, and small anions are located at the B site. Notably, some transition metals can serve as both A and X elements in different cases depending on the relative ionic radius and electronegativity, which has rarely been observed in traditional perovskites [19].
Figure I.5 shows the elemental constituents of thus far known antiperovskites.

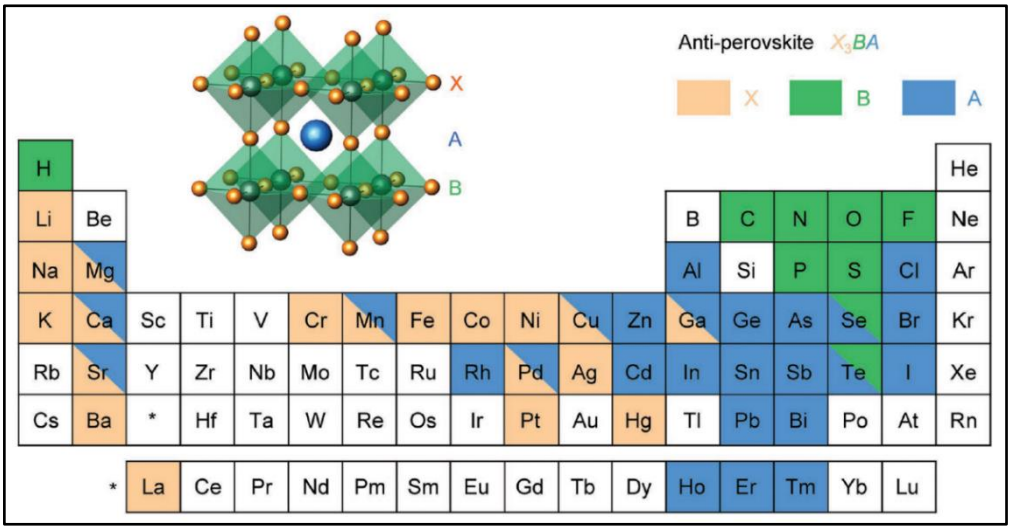

Figure I. 5: Crystal structure of a cubic antiperovskite and elemental constituents of thus far known antiperovskites X_3BA [19].

More specifically, Mn-based Antiperovskites structures have become one of the favored areas of materials research because they exhibit various exciting physical properties including giant magnetoresistances [20], piezomagnetism [21], giant negative thermal [22], magnetocaloric effect [23], and giant magnetostriction [24]. (Figure I.6) shows the Crystallography structure of Mn-based antiperovskites ($AXMn_3$) note that the Mn atom is located at the corners of the XMn_6 octahedron in $AXMn_3$.

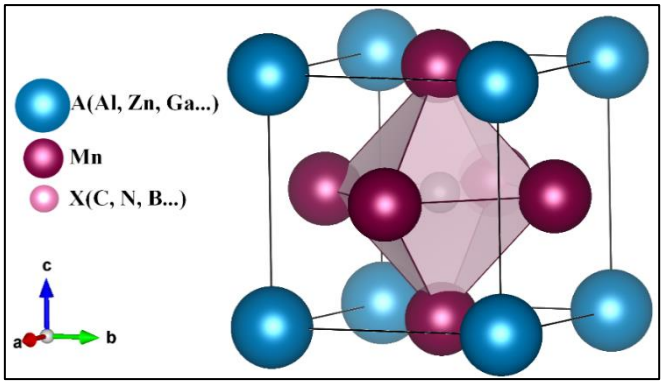

Figure I. 6: Crystallography structure of antiperovskites materials ($AXMn_3$).

I.2.2. Insulating, semiconductor, conductor, and superconducting properties

Materials in which the structure of perovskites are extremely interesting because of the enormous variety of solid-state phenomena they exhibit. These materials support an astounding variety of types from metallic, insulating, semiconductor, and semiconducting. Some have delocalized energy-band states, some have localized electrons, and others display transitions between these two types of behaviours. Many of the perovskites are magnetically ordered, and a large variety of magnetic structures can be found. Also, we can find this in the antiperovskites materials. The table (I.3) below provides a brief list of some well-studied perovskites and antiperovskites.

Table I. 3: Examples of different type of PVs and APVs materials.

Materials	Insulating	Metallic	Magnetic	semiconductor	Superconducting
Perovskites	$BaTiO_3$	$LaWO_3$	$LaMnO_3$	$KNbO_3$	$SrTiO_3$
Antiperovskites	$SnOSr_3$	$InCSc_3$	Mn_3GaC	Ca_3PN	$MgCNi_3$

I.2.3. Conditions of stability of the perovskite structure

I.2.3.1 Tolerance factor t

Victor Moritz Goldschmidt, developer of Goldschmidt classification of elements, first described this structure in his work on tolerance factors in 1926. Goldschmidt described that

stability of perovskite structures can be determined by the ionic radius of the individual species participating to form the structure by the following equation [25-26]:

$$t = \frac{r_A + r_X}{\sqrt{2}(r_B + r_X)} \quad \text{I.1}$$

Where *t* represents Goldschmidt's tolerance factor, and r_A, r_B and r_X represent the ionic radii of elements occupying A, B and X sites in the perovskite structure, respectively.

The same formula for tolerance factor and unit cell size from perovskites applies to antiperovskites as well, and just like perovskites, the properties of antiperovskites depend greatly upon the individual elements of the structure and it can be fine-tuned by varying the concentration of constituent elements in the structure.

In the ideal case where t = 1, the structure is cubic. As soon as one moves away from this value, the mesh undergoes the following distortions:

• t> 1: hexagonal distortion (ex: $BaTiO_3$, $NaNbO_3$)

• 0.95 <t <1: cubic structure (ex: $BaZrO_3$)

• 0.9 <t <0.95: rhombohedral distortion (ex: $RbTaO_3$, $KNbO_3$)

• 0.8 <t <0.9: orthorhombic distortion (ex: $PbTiO_3$, $GdFeO_3$, $LaMnO_3$)

I.2.3.2 The ionicity of anion-cation bonds

The second parameter which defines a criterion stability is the ionicity of the anion-cation bond. The ionic character of a ABX_3 composition is quantified from the differences in electronegativities given by the Pauling scale [27]:

$$\chi = \frac{(\chi_{A-X} + \chi_{B-X})}{2} \quad \text{I.2}$$

Where χ_{A-X} and χ_{B-X} : are the electronegativity differences between A and O, B and O, respectively. The perovskite structure is more stable when the bonds involved present a strong ionic character.

I.2.3.3 Electroneutrality

The electro-neutrality of the structure is also a fundamental element to take into account, in fact, the sum of the charges of the cations A and B must compensate for the charge of the oxygen anions. This results in load distributions such as: $A^{1+}B^{5+}X3$, $A^{2+}B^{4+}X3$, or $A^{3+}B^{3+}X3$ for chalcogenides perovskites, and for Halide perovskites $A^{+1}B^{+2}X3$.

I.2.3.4 Distortions of the structure

The ratio of the volume of the polyhedron of cation A (V_A) to that of cation B (V_B) is exactly 5. This ratio of V_A/V_B is a useful value which allows to characterize the degree of distortion of the perovskite structure. The smaller it is, the greater the structural distortion. An

example is $SrTiO_3$, whose structure is close to the ideal structure described above: a = 3,905 (Å), V_A = 49,623 ($Å^3$), V_B = 9,925 ($Å^3$), t = 1,002, V_A/V_B = 4,9998.

I.2.4. Physical properties and Some applications of PVs and APVs materials

There are several factors that make the perovskites particularly attractive as catalyst systems for research. One factor is that they form a large class of structurally similar compounds whose electronic properties can be varied in a controlled way. A second factor making the perovskites important as catalysts is that they are highly stable at high temperatures and in hostile chemical environments [28-29].

The technological uses of perovskite materials are extensive, and we will not attempt to review the field. we shall only briefly mention some of the common applications. They are used in memories, condensers [30], they are superconducting at temperatures relatively high [31], they transform mechanical pressure or heat in electricity (piezoelectricity) [32], accelerate chemical reactions (catalysts) [33] and suddenly change their electrical resistance when placed in a field magnetic (magnetoresistance) [34]. This variety is not only related to their chemical flexibility, but also to the greatest degree related to the complex character that the ions of transition metals play in certain coordinations with oxygen or halides [35-36].

Antiperovskites materials also present different possibilities of chemical combination. Therefore, these materials exhibit a variety of interesting physicochemical properties: from a large gap insulator [37] of a ferroelectric [38] to the superconductor [39-40], as they exhibit a structural change under pressure and temperature [41]. These different properties make antiperovskites materials very useful in different technological applications: in electro-optics [42], laser crystals [43], cutting tools [44], in the application of hard coatings. In addition, carbide and nitride based antiperovskites also exhibit interesting mechanical and magnetic properties, they have ferromagnetic, antiferromagnetic behavior [45]. It is concluded that its various technological applications of these materials make antiperovskites a vibrant and attractive field of research.

Important materials of PVs and APVs structures, possessing interesting properties and applications can be found in the tables (Table I.4- Table I.5).

Table I. 4: Properties and applications of some perovskites materials.

Compound	Physical property	Application
$BaTiO_3$	Ferroelectricity	[46]
$LiNbO_3$	Piezoelectricity	[47]
$KNbO_3$	Semiconductor	[48]
$SrTiO_3$	Superconductor	[49]
$LaMnO_3$	Giant magnetoresistance	[50]

Table I. 5: Properties and applications of some antiperovskites materials.

Compound	Physical property	Application
Ba_3GeO	Ferroelectricity	[51]
Mn_3NiN	Piezomagnetism	[52]
$SbNCa_3$	Semiconductor	[53]
$CdNNi_3$	Superconductor	[54]
Mn_3GaN	Giant magnetoresistance	[55]

I.3. References

[1] https://industryglobalnews24.com/maglev-technology-will-change-the-future

[2] https://inserbia.info/the-role-and-uses-of-magnetic-materials-in-the-industry/

[3] https://www.123rf.com/photo_25230295_creative-abstract-electronic-banking-and-finance-business-concept-set-of-plastic-credit-cards-isolat.html

[4] https://scitechdaily.com/science-made-simple-what-is-superconductivity/

[5] https://creativemarket.com/Raimundas/4398751-Electronic-circuit-board-close-up featuring-background-board-and-card

[6] Chadli, A., et al. "Ab Initio Study of Structural, Electronic, Magnetic and Magnetoelastic Properties of the Magnetoelectric h-YMnO 3 Semiconductor." *Journal of Electronic Materials* 50.2 (2021): 657-663.

[7]https://www.123rf.com/photo_57638355_macro-shooting-of-natural-mineral-stone-perovskite-crystals-titanium-ore-calcium-titanium-oxide-mine.html

[8] https://www.irocks.com/minerals/specimen/43725

[9] Wolfram, Thomas, and Sinasi Ellialtioglu. *Electronic and optical properties of d-band perovskites*. Cambridge University Press, 2006.

[10] Tilley, Richard JD. *Perovskites: structure-property relationships*. John Wiley & Sons, 2016.

[11] Chadli, Abdelhakim, et al. "Structural and anisotropic elastic properties of hexagonal YMnO3 in low symmetry determined by first-principles calculations." *Solid State Phenomena*. Vol. 297. Trans Tech Publications Ltd, 2019.

[12] Cheriet, Abderrahmane, et al. "First-principles study of structural, electronic, optical and elastic properties of cadmium based Fluoro-Perovskite MCdF3 (M= Rb, Tl)." *Solid State Phenomena*. Vol. 297. Trans Tech Publications Ltd, 2019.

[13] Benmalem, Y., et al. "Investigation of Transport Properties of Some Superconductor Nickel-Based Antiperovskite XNNi 3 (X= Mg, Al, Cu, Zn, Ga, Ag, Cd, In, Sn, Sb, Pt and Pb)." *Journal of Superconductivity and Novel Magnetism* 31.11 (2018): 3485-3501.

[14] Khandy, Shakeel Ahmad, et al. "Electronic structure, magnetism and elastic properties of inverse perovskite carbide: A first principles study." *Physica B: Condensed Matter* 578 (2020): 411839.

[15] Huang, Yun-Hui, et al. "Double perovskites as anode materials for solid-oxide fuel cells." *Science* 312.5771 (2006): 254-257

[16] Lamrani, Nouara. *Synthèse et caracterisation de matériaux dielectriques à structures perovskite complexe de type Ca1-xAxTi1-y bY03 (A= Sr, B= Zr,...)*. Diss. Universite Mouloud MAMMERI Tizi-Ouzou, 2011

[17] Hu, Jun, Liang Yan, and Wei You. "Two-dimensional organic–inorganic hybrid Perovskites: a new platform for optoelectronic applications." *Advanced Materials* 30.48 (2018): 1802041.

[18] Olsson, Emilia, Xavier Aparicio-Anglès, and Nora H. de Leeuw. "Ab initio study of vacancy formation in cubic LaMnO3 and SmCoO3 as cathode materials in solid oxide fuel cells." *The Journal of chemical physics* 145.1 (2016): 014703.

[19] Wang, Yonggang, et al. "Antiperovskites with exceptional functionalities." *Advanced Materials* 32.7 (2020): 1905007.

[20] Kim, W. S., et al. "Close correlation among lattice, spin, and charge in the manganese-based antiperovskite material." *Solid state communications* 119.8-9 (2001): 507-510.

[21] Zemen, J., Z. Gercsi, and K. G. Sandeman. "Piezomagnetism as a counterpart of the magnetovolume effect in magnetically frustrated Mn-based antiperovskite nitrides." *Physical Review B* 96.2 (2017): 024451.

[22] Qu, B. Y., and B. C. Pan. "Nature of the negative thermal expansion in antiperovskite compound Mn 3 ZnN." *Journal of Applied Physics* 108.11 (2010): 113920

[23] Alaoui, Y. Charif, et al. "Magnetocaloric effect in metallic antiperovskite Mn3InC compound: Ab-initio study and Monte Carlo simulations." *Solid State Communications* 309 (2020): 113841.

[24] Shibayama, T., and K. Takenaka. "Giant magnetostriction in antiperovskite Mn3CuN." *Journal of applied physics* 109.7 (2011): 07A928.

Chapter I: Literature notes about perovskites

[25] Goldschmidt, V. M. "The laws of crystal chemistry." *Naturwissenschaften* 14.21 (1926): 477-485.

[26] Roth, Robert S. "Classification of Perovskite and Other ABOs-Type." *Journal of Research of the National Bureau of Standards* 58 (1957): 75.

[27] DJERMOUNI, Mostefa. "Electronic Structure and Magnetic Properties in Perovskite-Related Materials." PhD diss., 2015.

[28] Hazen, Robert M. "Perovskites." *Scientific American* 258.6 (1988): 74-81.

[29] Desgardin, G., H. Bali, and B. Raveau. "Ceramiques composites a base de perovskites et pyrochlores au plomb PZN (PbZn13Nb23) O3, PFN (PbFe12Nb12) O3 et PMN (PbMg13Nb23) O3 pour condensateurs multicouches a haute constante dielectrique." *Materials Chemistry and Physics* 8.5 (1983): 469-491.

[30] Rubel, M. H. K., et al. "Newly synthesized A-site ordered cubic-perovskite superconductor (Ba0. 54K0. 46) 4Bi4O12: A DFT investigation." *Physica C: Superconductivity and its Applications* 574 (2020): 1353669.

[31] Zheng, Ting, et al. "Recent development in lead-free perovskite piezoelectric bulk materials." *Progress in materials science* 98 (2018): 552-624.

[32] Laugel, Guillaume, et al. "Preparation and characterisation of metal oxides supported on SBA-15 as methane combustion catalysts." *Comptes Rendus Chimie* 12.6-7 (2009): 731-739.

[33] Hu, Chun-lian, et al. "Theoretical study on the positive magnetoresistance in perovskite oxide p–n junctions." *Solid state communications* 149.7-8 (2009): 334-336.

[34] Ha, Son-Tung, et al. "Metal halide perovskite nanomaterials: synthesis and applications." *Chemical science* 8.4 (2017): 2522-2536

[35] Schileo, Giorgio, and Giulia Grancini. "Halide perovskites: current issues and new strategies to push material and device stability." *Journal of Physics: Energy* 2.2 (2020): 021005.

[36] Fang, Yuan, and Jennifer Cano. "Higher-order topological insulators in antiperovskites." *Physical Review B* 101.24 (2020): 245110.

[37] Garcia-Castro, Andrés Camilo, Jorge Hernan Quintero Orozco, and Carlos José Paez Gonzalez. "Hybrid-improper ferroelectric behavior in Ba 3 SiO/Ba 3 GeO oxide antiperovskite superlattices." *The European Physical Journal B* 92.9 (2019): 1-5.

[38] Oudah, Mohamed, et al. "Superconductivity in the antiperovskite Dirac-metal oxide Sr 3− x SnO." *Nature communications* 7.1 (2016): 1-6.

[39] Uehara, Masatomo, et al. "New antiperovskite superconductor ZnNNi3, and related compounds CdNNi3 and InNNi3." *Physica C: Superconductivity and its applications* 470 (2010): S688-S690.

[40] Ciftci, Yasemin O., Meryem Evecen, and İrem O. Alp. "Pressure effects on electronic, elastic, and vibration properties of metallic antiperovskite PbNCa 3 by ab initio calculations." *Journal of Molecular Modeling* 27.1 (2021): 1-9.

[41] Khalladi, R., et al. "Magnetic properties study of the anti-perovskite Mn3CuN compound by Monte Carlo simulations." *Solid State Communications* 290 (2019): 42-48.

[42] Minohara, Makoto, et al. "Growth of antiperovskite oxide Ca3SnO films by pulsed laser deposition." *Journal of Crystal Growth* 500 (2018): 33-37

[43] Hui, Zhenzhen, et al. "Synthesis and Physical Properties of Antiperovskite CuNFe3 Thin Films via Solution Processing for Room Temperature Soft-Magnets." *Coatings* 10.3 (2020): 270.

[44] Çakır, Ö., et al. "Dynamics of nonergodic ferromagnetic/antiferromagnetic ordering and magnetocalorics in antiperovskite Mn 3 SnC." *Physical Review B* 96.1 (2017): 014436.

[45] Benhouria, Y., et al. "Carbides-anti-perovskites Mn3 (Sn, Zn) C: Potential candidates for an application in magnetic refrigeration." *Physica E: Low-dimensional Systems and Nanostructures* 124 (2020): 114317.

[46] Shen, Zhengbo, et al. "BaTiO3–BiYbO3 perovskite materials for energy storage applications." *Journal of Materials Chemistry A* 3.35 (2015): 18146-18153.

[47] Jackel, J. L., and C. E. Rice. "Topotactic LiNbO3 to cubic perovskite structural transformation in LiNbO3 and LiTaO3." *Ferroelectrics* 38.1 (1981): 801-804.

[48] Wermuth, Tiago Bender, et al. "Microwave-synthesized KNbO3 perovskites: photocatalytic pathway on the degradation of rhodamine B." *Ceramics International* 45.18 (2019): 24137-24145.

[49] Gor'kov, Lev P. "Phonon mechanism in the most dilute superconductor n-type SrTiO3." Proceedings of the National Academy of Sciences 113.17 (2016): 4646-4651.

[50] Yin, Wei-Guo, and Ruibao Tao. "Effective-medium theory of the giant magnetoresistance in magnetic granular samples and doped LaMnO 3 perovskites." *Physical Review B* 62.1 (2000): 550.

[51] Garcia-Castro, Andrés Camilo, Jorge Hernan Quintero Orozco, and Carlos José Paez Gonzalez. "Hybrid-improper ferroelectric behavior in Ba 3 SiO/Ba 3 GeO oxide antiperovskite superlattices." *The European Physical Journal B* 92.9 (2019): 1-5.

[52] Na, Yuanyuan, et al. "Preparation and properties of antiperovskite Mn3NiN thin film." *Materials Letters* 65.23-24 (2011): 3447-3449.

[53] Bilal, M., et al. "Thermoelectric properties of SbNCa3 and BiNCa3 for thermoelectric devices and alternative energy applications." *Computer Physics Communications* 185.5 (2014): 1394-1398.

[54] Uehara, Masatomo, et al. "New antiperovskite superconductor ZnNNi3, and related compounds CdNNi3 and InNNi3." *Physica C: Superconductivity and its applications* 470 (2010): S688-S690.

[55] Sakakibara, H., et al. "Magnetic properties and anisotropic magnetoresistance of antiperovskite nitride Mn3GaN/Co3FeN exchange-coupled bilayers." *Journal of Applied Physics* 117.17 (2015): 17D725.

"A person who never made a mistake never tried anything new."

-Albert Einstein

Chapter II: Methods & Concepts

Chapter II: Methods & concepts

II.1. Introduction

Towards the end of the 19th century, it was believed that the evolution of physical systems could be described within the framework of classical mechanics. However, some facts remained poorly understood. They would lead to questioning this belief, and to profoundly modify the basic concepts of physics. Therefor a new framework was needed which is quantization rules.

The use of "quantization rules" within the framework of classical mechanics remained unsatisfactory. In 1925, independently of each other, W. Heisenberg and E. Schrodinger formulated two more systematic quantum theories, apparently different but which have been shown to be equivalent. On this basis, thanks to the efforts of these two scientists, P. Dirac, J. von Neumann, N. Bohr, M. Born and others, a new Mechanics was created: Quantum Mechanics.

This new Mechanic:

• Admits classical mechanics as a limiting case, for systems of large dimension and large mass.

• Leads to precise quantification rules, not imposed a priori, but consequences of theory.

• “Explains” why matter and electromagnetic radiation can, as L. Broglie (1924) discovered, behave sometimes like particles and sometimes like waves.

Quantum mechanics has helped explain many hitherto mysterious physical properties.

Based on the laws of quantum mechanics we can describe and explain the physical properties of interacting electron systems.

In 1926, Erwin Schrodinger published his famous equation that predicts behavior of particles in quantum system. However, because of the large number of interactions, solving the Schrödinger’s equation becomes a very difficult, even impossible task. For this, techniques and approximations have continued to develop since the first approximation proposed by Born-Oppenheimer in 1927, the second approximation proposed by Hartree 1928, the third approximation proposed by Hartree Fock in 1930. and whose goal is to simplify the solution of the characteristic equation of the system with several particles (Many Body Problems).

Chapter II: Methods & concepts

Pierre Hohenberg and Walter Kohn published a Physical Review Paper, where they stated two fundamental theorems which gave birth to modern Density Functional Theory (DFT). Hohenberg, Kohn and Sham established a logically rigorous DFT of the quantum ground state based on quantum mechanics, we begin a review of some key ideas from quantum mechanics that underlie DFT. Our goal here is not to present a complete derivation of the techniques used in DFT. Instead, our goal is to give a clear, brief, introductory presentation of the most basic important equations for DFT. For the full story, there are a number of excellent texts devoted to quantum mechanics listed in the Further Reading section at the end of the chapter.

II.2. Schrödinger's equation

According to Erwin Schrödinger (1887-1961) [1], the description of the quantum dynamics of a non-relativistic particle of mass m, is based on a mathematical object of wave nature called the wave function $\psi(\boldsymbol{r}, t)$.

The problem comes down to solving a wave equation of the form:

$$\left(-\frac{\hbar^2}{2\mathrm{m}}\boldsymbol{\nabla}^2 + \mathrm{V}(\mathbf{r},\mathrm{t})\right)\psi(\mathbf{r},\mathrm{t}) = \mathrm{i}\hbar\frac{\partial}{\partial \mathrm{t}}\psi(\mathbf{r},\mathrm{t}) \qquad \text{II-(1)}$$

For a system of isolated particles, the total energy E is constant. The system is then said to be in a stationary quantum state. The time-independent Schrödinger equation [2-3] describes these states and the energies with which they are associated. If the system is made up of atoms or molecules we can then write:

$$\mathrm{H}\psi(\{\mathbf{r_i}\},\{\mathbf{R_I}\}) = \mathrm{E}\psi(\{\mathbf{r_i}\},\{\mathbf{R_I}\}) \qquad \text{II-(2)}$$

Where H is the Hamiltonian operator of the system, $\psi(\{\mathbf{r_i}\},\{\mathbf{R_I}\})$ is the wave function with several particles, where the set $\{r_i\}$ contains the variables describing the electrons and $\{R_I\}$ those describing the nuclei, E is the energy of the described ground state by wave function.

Such as: $$\mathrm{H} = \mathrm{T_n} + \mathrm{T_e} + \mathrm{V_{n-e}} + \mathrm{V_{e-e}} + \mathrm{V_{n-n}} \qquad \text{II-(3)}$$

Where:

T_n : Kinetic energy of N nuclei of mass M_n.

T_e : Kinetic energy of M electrons of mass m_e.

V_{n-e} : Attractive nucleus-electron Coulomb interaction.

V_{e-e} : Repulsive electron-electron Coulomb interaction.

V_{n-n} : Coulomb repulsive nucleus-nucleus interaction.

So:

$$H = \sum_{i=1}^{n} \frac{-\hbar^2 \nabla_i^2}{2m} + \sum_{I=1}^{N} \frac{-\hbar^2 \nabla_I^2}{2M_I} - \sum_{i=1}^{n} \times \sum_{I=1}^{N} \frac{Z_I k e^2}{|\mathbf{r_i} - \mathbf{R_I}|} + \frac{1}{2} \sum_{i,i \neq j} \frac{k e^2}{|\mathbf{r_i} - \mathbf{r_j}|} + \frac{1}{2} \sum_{I \neq J} \frac{Z_I Z_J k e^2}{|\mathbf{R_I} - \mathbf{R_J}|} \quad \text{II-(4)}$$

The first term corresponds to the kinetic energy of the electrons, the second term corresponds to the kinetic energy of the nuclei, the third term corresponds to the electron-nuclei interaction energy, the fourth term corresponds to the electron-electron interaction energy and the last term corresponds to the nuclei-nuclei interaction energy. However, the electron-electron interaction energy is hard to calculate. At this point, some approximations could be made to solve this Hamiltonian.

To facilitate calculations, it is more convenient to work with atomic units (a. u) than with International System (IS) units, these units are shown in table II.2.

Table II. 1: The atomic units used in DFT.

Sizes	Symbol or expression in IS	Value in IS	Atomic unit (a. u)
Electron mass	m_e	$9{,}1094 \times 10^{-31}$ kg	1 a. u
Electron charge	e	-1.6022×10^{-19} C	1 a. u
Length (Bohr radius)	$a_0 = \frac{4\pi\varepsilon_0\hbar}{m_e e^2}$	$5{,}2918 \times 10^{-11}$ m	1 a. u = 1Bohr
Strength	$F = \frac{E_0}{a_0}$	$8{,}2387 \times 10^{-8}$ N	1 a. u =1Hartree/Bohr
Energy	$E_0 = \frac{\hbar^2}{m_e a_0^2}$	$4{,}3597 \times 10^{-18}$ J	1 a. u = 1 Hartree
Action	$\hbar = \frac{h}{2\pi}$	$1{,}0546 \times 10^{-34}$ J. s	1 a. u

II.3 Born-Oppenheimer approximation

Let us imagine a situation where we would like to describe the properties of some well-defined collection of atoms, you could think of an isolated molecule or the atoms defining the crystal of an interesting mineral. One of the fundamental things we would like to know about these atoms is their energy and, more importantly, how their energy changes if we move the atoms around. To define where an atom is, we need to define both where its nucleus is and

where the atom's electrons are [4]. Born Oppenheimer approximation is based on the fact that the nuclei are much heavier than the electrons. This means, roughly speaking, that electrons respond much more rapidly to changes in their surroundings than nuclei can. As a result, we can split our physical question into two pieces. First, we solve, for fixed positions of the atomic nuclei, the equations that describe the electron motion. For a given set of electrons moving in the field of a set of nuclei, we find the lowest energy configuration, or state, of the electrons. The lowest energy state is known as the ground state of the electrons, and the separation of the nuclei and electrons into separate mathematical problems is the Born– Oppenheimer approximation [5].

As a result, the electronic relaxation is instantaneous with respect to the movement of the nuclei. Then we can write the wave function of the system as the product of two wave functions; one for nuclei and the other for electrons which is the electronic wave function. Thus, the potential energy V_{n-n} becomes a constant (We can always introduce T_N and V_{n-n} to tackle the problem of network vibrations *(phonons).*

$$\psi(\{\mathbf{r_i}\},\{\mathbf{R_I}\}) = \psi_e(\{\mathbf{r_i}\},\{\mathbf{R_I}\}) \times \varphi_N(\{\mathbf{R_I}\}) \qquad \text{II-(5)}$$

Where $\psi_e(\{r_i\},\{R_I\})$: is the electron wave function (we are interested in the electronic wave function which must satisfy the equation II-(2)) and $\varphi_N(\{R_I\})$ is the nuclear wave function.

We thus neglect the kinetic energy T_N of the nuclei and the potential energy nucleus-nuclei becomes a constant, then the Hamiltonian of the system can be reduced to an electronic Hamiltonian:

$$H_e = T_e + V_{n-e} + V_{e-e} = -\frac{1}{2}\sum_{i=1}^{n} \boldsymbol{\nabla_i^2} - \sum_{i=1}^{n}\sum_{I=1}^{N} \frac{Z_I}{|\mathbf{R_I}-\mathbf{r_i}|} + \sum_{i}^{n}\sum_{j>i}^{n} \frac{1}{|\mathbf{r_i}-\mathbf{r_j}|} \qquad \text{II-(6)}$$

If we replace equations II-(5) and II-(6) in equation II-(2), we get:

$$H_e\psi_e(\{\mathbf{r_i}\},\{\mathbf{R_I}\}) = E_e\psi_e(\{\mathbf{r_i}\},\{\mathbf{R_I}\}) \qquad \text{II-(7)}$$

All the *ab initio* methods are based on these last two equations for the calculation of the electronic structure.

II.4. Hartree approximation

Chapter II: Methods & concepts

Hartree [6] proposed the mean field hypothesis which states that each electron evolves in an effective potential generated by nuclei and other electrons. In Hartree's approximation, the total wave function $\psi_e(\mathbf{r_1}, \mathbf{r_2} \ldots, \mathbf{r_n})$ is replaced by a direct product of molecular orbitals which contains the spin information, or simpler spin-orbitals:

$$\psi_e(\mathbf{r_1}, \mathbf{r_2} \ldots, \mathbf{r_n}) = \prod_{i=1}^{n} \psi_i(\mathbf{r_i}) \qquad \text{II-(8)}$$

Equation II-(7) is then transformed into a system of mono-electronic equations:

$$\mathrm{H_H}\psi_i(\mathbf{r_i}) = \boldsymbol{\varepsilon_i}\psi_i(\mathbf{r_i}) \qquad \text{II-(9)}$$

The electronic Hamiltonian is written in the following form:

$$H_H = \sum_{i=1}^{n} \frac{-\hbar^2 \nabla_i^2}{2m} + \frac{1}{2}\sum_{i,i\neq j} \frac{ke^2}{|\boldsymbol{r_i} - \boldsymbol{r_j}|} - \sum_{i=1}^{n} \times \sum_{I=1}^{N} \frac{Z_I ke^2}{|\boldsymbol{r_i} - \boldsymbol{R_I}|} \qquad \text{II-(10)}$$

The first term corresponds to the kinetic energy of the electron, the second represents the potential that the electron experiences (Hartree potential), and the third term is the potential created by the nuclei.

The consequences of this approximation are:

- The total Colombian repulsion is overestimated.
- The Pauli principle is not respected.
- We do not take into account the effects of exchange and correlation.

To correct this, Hartree and Fock proposed to express the multielectron wave function as a Slater determinant.

II.5. Hartree-Fock approximation

In its traditional statement, Hartree-Fock theory does not use the formalism of the second quantization. To get around the polyelectronic problem and to get closer to the one electron problem, we use the monoelectronic approximation which consists in considering each electron as being independent but undergoing an effective potential, which must consider all the electronic interactions.

The electronic system in Hartree's approximation is not fully described.

In 1930, Fock [7] showed that the Hartree wave function violates the principal exclusion of Pauli because it is not antisymmetric to the exchange of two electrons. He replaced the wave function Ψ ($r_1, r_2 \ldots\ldots r_n$) with a Slater determinant:

$$\psi_e = \psi_{SD} = \frac{1}{\sqrt{N!}} \begin{vmatrix} \psi_1(\mathbf{r}_1) & \psi_2(\mathbf{r}_1) & \cdots & \psi_N(\mathbf{r}_1) \\ \psi_1(\mathbf{r}_2) & \psi_2(\mathbf{r}_2) & \cdots & \psi_N(\mathbf{r}_2) \\ \vdots & \vdots & \ddots & \vdots \\ \psi_1(\mathbf{r}_N) & \psi_2(\mathbf{r}_N) & \cdots & \psi_N(\mathbf{r}_N) \end{vmatrix} \qquad \text{II-(11)}$$

Where $\frac{1}{\sqrt{N!}}$:is the normalization constant.

Each wave function ψ_i is called orbital spin because it is made up of two parts: a space orbital function and the other is a spin function (up or down). This maneuver respects the nature of the electrons (*fermions*), so the Pauli principle is respected. Slater's determinant is determined using the variational principle.

The consequences of the Hartree-Fock approach can be summarized in the following points:

- it obeys the principle of Pauli.
- there is no self-interaction.
- it introduces the exchange effect.
- it does not consider the correlation effect.

II.6. Density Functional Theory DFT

The quantum many bodies problem obtained after the first level approximation (*Born-Oppenheimer*) is much simpler than the original one, but still far too difficult to solve. Several methods exist to reduce equation II-(6) to an approximate but tractable form.

The approximations developed up to the 1960s were all based on the multi-electronic wave function. The cumbersome calculations by these approximations, the imprecision of the results and the performance of unsuitable calculation means have pushed the researchers towards new methods. Although its history goes back to the early thirties of the 20th century, DFT has been formally established in 1964 by two theorems due to Pierre Hohenberg and Walter Kohn [8], a new idea was proposed which consists in replacing the very bulky multi-electronic wave function, by electron density, a simpler and more manageable function. This idea is based on the model of Hewellyn Thomas [9] and Fermi [10] (1927). This theory was named DFT (*Density Functional theory*).

Chapter II: Methods & concepts

II.6.1. Hohenberg and Kohn theorem

The traditional formulation of the two theorems of Hohenberg and Kohn is as follows:

II.6.1.1. First theorem

The first theorem shows that there is a one-to-one correspondence between the ground-state density $\rho(\vec{r})$ of a many-electron system (atom, molecule, solid) and the external potential $V_{ext.}$ It demonstrates that the ground state energy of a system with several electrons in the external potential is a unique functional of the electron density $n(\mathbf{r})$, written as:

$$E[n(\mathbf{r})] = T[n(\mathbf{r})] + \int n(\mathbf{r})\, V_{ext}(\mathbf{r})\, d^3r \; + V_{ee}[n(\mathbf{r})] = \int n(\mathbf{r})\, V(\mathbf{r})\, d^3\boldsymbol{r} + F_{HK[n]} \qquad \text{II-(12)}$$

Where $F_{HK}[n(\mathbf{r})] = T[n(\mathbf{r})] + V_{ee}[n(\mathbf{r})]$:is the universal functional of Hohenberg and Kohn does not depend on the potential which acts on the system. This functional is not exactly known.

II.6.1.2. Second theorem:

The second theorem shows, in accordance with the variational principle, that the total energy functional of any multi-particle system has a minimum which corresponds to the ground state and the density of particles of the ground state.

$$\mathrm{E}_0 < E[\mathrm{n}(\mathbf{r})] \qquad \text{II-(13)}$$

Where n(**r**) is the exact electron density of the ground state system.

Unfortunately, the Hohenberg and Kohn functional is not known in practice. This problem can be worked around by approximations. The most widely answered is that of Kohn-Sham.

II.6.2. The Kohn-Sham approach

The Hohenberg and Kohn functional is not known in practice. This problem can be worked around by approximations. The most widely answered is that of Kohn-Sham [11].

The stated approximations could not have the potential to fully describe the many body systems. The electrons have both the exchange and correlation properties. When the two electrons change their positions, the interaction energy between these electrons changes that is the exchange property. Also, the motion of every other electron in the system affects each electron that is the correlation property. The revolution and the discovery of DFT come with the two papers written by Hohenberg- Kohn [12] and Kohn-Sham that consider the total electron density to solve the Schrödinger equation like Khon-Sham equations.

The energy of the ground state of the real system E_0 is written:

$$E_0[n(\mathbf{r})] = T_0[n(\mathbf{r})] + U_0[n(\mathbf{r})] \qquad \text{II-(14)}$$

Where E_0: the electronic contribution to the total energy of the ground state of the real system.

T_0: the kinetic energy of the real system.

U_0: the potential energy of the real system (external and Hartree-Fock): $U_0 = U_{HF} + U_{ext}$.

Also, the energy of the fictitious system is expressed by:

$$E[n(\mathbf{r})] = T[n(\mathbf{r})] + U_H[n(\mathbf{r})] + U_{ext}[n(\mathbf{r})] \qquad \text{II-(15)}$$

With:

E: is the electronic contribution to the total energy of the fictitious system.

T: is the kinetic energy

U_H: is Hartree's potential energy.

U_{ext}: is the external potential energy.

Subtracting II-(16) and (17) gives:

$$E_0 - E = T_0 - T + (U_{HF} - U_H) \qquad \text{II-(16)}$$

This difference is only the energy of electronic correlation expressed by:

$$U_C = T_0 - T \qquad \text{II-(17)}$$

Also, the exchange energy is written in the following form:

$$U_X = -(U_{HF} - U_H) \qquad \text{II-(18)}$$

We can define the energy of exchange and correlation by:

$$U_{XC} = U_C - U_X \qquad \text{II-(19)}$$

By replacing II-(21) in II-(16) we find the expression of the energy of the real system:

$$E_0[n(\mathbf{r})] = T[n(\mathbf{r})] + U_H[n(\mathbf{r})] + U_{XC}[n(\mathbf{r})] + U_{ext}[n(\mathbf{r})] \qquad \text{II-(20)}$$

The Hohenberg and Kohn functional (equation II-16) is written:

$$F_{HK}[n(\mathbf{r})] = T + U_H + U_{XC} \qquad \text{II-(21)}$$

Chapter II: Methods & concepts

Applying the second theorem of Hohenberg and Kohn, the ground-state electron density is determined using a new Hamiltonian, said from Kohn-Sham:

$$H_{KS} = T + U_H + U_{XC} + U_{ext} \qquad \text{II-(22)}$$

The Kohn-Sham equations are:

$$H_{KS}\psi_i = \varepsilon_i\psi_i \qquad \text{II-(23)}$$

With ψ_i : is the wave function of the i^{th} electron.

So far, the DFT is an exact method but for the DFT and the equations of Kohn Sham become usable in practice, we need to propose a formulation of $E_{XC}[n(r)]$and for that, we must go through an approximation.

II.7. Approximations for the exchange and correlation term

The exchange-correlation functional is a useful consideration in the DFT.

II.7.1. Local density approximation (LDA)

Despite E_{XC} is very complex, approaches have been performed to define it. One approach for the exchange-correlation functional is the Local Density Approximation (LDA) [13] that accounts the exchange-correlation energy as simply an integral over all space with the same exchange-correlation energy density $\varepsilon_{XC}^{LDA}[n(\mathbf{r})]$ as given in the following equation:

$$E_{XC}^{LDA}([n(\mathbf{r})]) = \int n(\mathbf{r})\, \varepsilon_{XC}^{LDA}[n(\mathbf{r})]d\mathbf{r} \qquad \text{II-(24)}$$

Where $\varepsilon_{XC}^{LDA}[n(\mathbf{r})]$: is the exchange-correlation energy density (energy / particle) of a uniform electron gas of density n (r).

The exchange-correlation functional can be divided into an exchange contribution $\varepsilon_x(n(\mathbf{r}))$and a correlation contribution $\varepsilon_c(n(\mathbf{r}))$:

$$\varepsilon_{XC}^{LDA}(n(\mathbf{r})) = \varepsilon_x(n(\mathbf{r})) + \varepsilon_c(n(\mathbf{r})) \qquad \text{II-(25)}$$

With $\varepsilon_X\big(n(\mathbf{r})\big) = \frac{3}{4}\left(\frac{3}{\pi}\right)^{\frac{1}{3}} n(\mathbf{r})^{\frac{1}{3}}$ from the Dirac exchange functional.

For the correlation part, no such explicit analytical expression is known. Several different parameterizations have been proposed since the beginning of the 1970s; Barth and Hedin (1972), Vosko et al (1980), and Perdew and Zunger (1981) [14], etc. The most accurate results are based on the quantum Monte Carlo simulations of Ceperley and Alder [15].

The local density approximation (LDA) works well for systems where the density varies slowly. It is less good for systems of more inhomogeneous density, for this it is necessary to make the description of the exchange-correlation energy more precise in order to be able to represent the system correctly.

II.7.2. Generalized gradient approximation (GGA)

LDA takes the density as a constant but in some cases this approximation is not valid, and the variation of the density should be included. So, another approach for the exchange-correlation functional is called Generalized Gradient Approximation (GGA) [16-17] that depends on the gradient of the density (f(n(r), ∇(n(r))) as given in Equation 28.

$$\mathrm{E}_{\mathrm{xc}}^{\mathrm{GGA}}[\mathrm{n}(\mathbf{r})] = \int \varepsilon_{XC}^{GGA}[\mathrm{n}(\mathbf{r}), \boldsymbol{\nabla}\mathrm{n}(\mathbf{r})] \,.\, \mathrm{n}(\mathbf{r})\mathrm{d}\mathbf{r} \qquad \text{II-(26)}$$

Where ε_{XC}^{GGA} :is the correlation exchange energy density.

There are different GGA methods that take different f(n(r), ∇(n(r)) such as Perdew-Wang (PW91) [18], Perdew-Burke-Ernzerhof (PBE) [19], etc. The GGA with Wu-Cohen (WC) functional has been employed for the exchange- correlation calculations within this thesis.

II.8. The DFT + U method

The DFT +U method is a pragmatic and effective approach for calculating the ground-state properties of strongly correlated systems, and linear-response calculations are widely used to determine the requisite Hubbard [20] parameters from first principles.

LDA and GGA are the mostly used approximations for the exchange-correlation functional. Another approach is LDA+U or GGA+U approach that's based on LDA or GGA type functional with an additional orbital dependent interaction parameter. The interaction parameter is essential for highly localized orbitals as d and f orbitals. The U parameter gives better results than LDA or GGA.

The total energy of the system can be summarized by the following expression [21]:

$$E^{GGA+U} = E^{GGA} + \frac{\bar{U}-\bar{J}}{2}\sum_{\sigma}\left[\left(\sum_{m} n^{\sigma}_{m,m}\right) - \left(\sum_{m,m} n^{\sigma}_{m,m}.n^{\sigma}_{m,m}\right)\right] \qquad \text{II-(27)}$$

From where:

$\bar{U}$ *and* $\bar{J}$: are moderately spherical matrix elements of Coulomb interactions,

And n: is the occupation matrix of 3d states obtained by projection of the wave function onto 3d atomic type states (m or m'=-2, -1, 0, 1, 2 indicates the different states d, while σ = 1 or -1 indicates the spin).

Note that we express the occupancy matrix in an explicit representation of spin and orbit. An efficient interaction parameter$U_{eff} = \bar{U} - \bar{J}$, or simply U, can be introduced. The calculated total energies are insensitive to $\bar{J}$ when U_{eff} is fixed [22].

II.9. Calculation methods

II.9.1. The base of plane waves (PW)

plane waves form a “complete” basis set; however, they “never” converge due to the rapid oscillations of the atomic wave functions χ close to the nuclei.

The plane wave decomposition of $\varphi_j^k(\boldsymbol{r})$ wave functions consist in expressing these wave functions using Fourier series:

$$\varphi_j^k(\mathbf{r}) = \Omega^{-1/2}\sum_G C_j^k(\mathbf{G})e^{i(\boldsymbol{K}+\mathbf{G})\mathbf{r}} \qquad \text{II-(28)}$$

Plane wave bases, associated with periodic boundary conditions, are often suitable for the study of solids since they by construction satisfy Bloch's theorem.

Representing the wave function in a plane wave base presents two major problems, even with the use of critical energy. First, to have a correct representation of the electronic wave function one has to use an infinite number of plane waves, which is impossible. Then the choice of number of plane waves to use is truncated by a cut-off energy E_{cut} such that:

$$\frac{\hbar^2}{2m}|K+G| < E_{cut} \qquad \text{II-(29)}$$

To determine this very important parameter of calculation one must always make a study of convergence. The second problem is that the valence electron wave function exhibits rapid oscillations near the nucleus, so to have an exact description of these oscillations it is necessary to take many plane waves, something which is impracticable., to solve this problem we replace

the Colombian potential of nuclei and core electrons felt by valence electrons by a pseudo potential.[23].

II.9.2. Pseudopotential method (PP):

A necessary choice in solving the Kohn-Sham equations concerns the method that should be used to deal with the electron-nucleus interaction. We must distinguish between two classes of electrons with different properties:

i. those who actively participate in the bonding of atoms called valence electrons. It is these electrons that first determine the physical properties of materials.
ii. those which are strongly localized near the nucleus, called the core electrons. These do not participate in binding and thus they can be treated as frozen orbitals, i.e., will not be modified during chemical reactions.

Core electrons have two main effects:

• screen the charge of the nucleus: far from the nucleus in the outer layers, the apparent charge of the nucleus is the sum of the charge of the protons plus those of the core electrons.

• and cause strong oscillations on the wave functions of valence electrons.

Two classes of methods exist for the calculation of the electron-nucleus potential:

• the all-electron methods (Full potential + Muffin-Tin) which explicitly process all electrons in the system,

• and the pseudopotential methods (Empirical + Ab-initio), which explicitly only deals with valence electrons.

The formalism of the pseudopotential method consists in replacing the atomic system {naked nucleus + electrons} by a system {[naked nucleus + core electrons] + valence electrons} equivalent to {ionic core + valence electrons}.

[24-25].

• Is the introduction of the pseudopotential completely innocent?

• What do you do if you are interested in information that is inherently contained in the region near the nucleus (hyperfine fields for instance, or core level excitations)?

II.9.3. The APW method

Although the pseudopotential method is extremely useful, there are reasons why alternatives could be attractive. Therefore, we will search for a basis set that uses other functions than plane waves, and that does not require the introduction of a pseudopotential. Such a basis set will have to be more efficient, but of course we do not want it to be biased. Our first example of this will be the Augmented Plane Wave (APW) basis set. Right from the beginning it has to be said that the APW-method itself is of no practical use any more today. But for didactical reasons it is advantageous to discuss APW first. The ideas that lead to the APW basis set are very similar to what made us to introduce the pseudopotential. In the region far away from the nuclei, the electrons are more or less 'free'. Free electrons are described by plane waves [26]. Close to the nuclei, the electrons behave quite as they were in a free atom, and they could be described more efficiently by atomic like functions. Space is therefore divided now in two regions:

•Around each atom11 a sphere with radius Rα is drawn (call it Sα). Such a sphere is often called a muffin tin sphere,

•The part of space occupied by the spheres is the muffin tin sphere. The remaining space outside the spheres is called the interstitial region (call it I).

One augmented plane wave (APW) used in the expansion of $\phi(r)$ is defined as:

$$\phi(r) = \begin{cases} \varphi_i(\boldsymbol{r}) = \frac{1}{\Omega^{\frac{1}{2}}} \sum_G C_G e^{i(\boldsymbol{k}+\boldsymbol{G})\boldsymbol{r}}, & r > I \\ \varphi_s(\boldsymbol{r}) = \sum_{lm} A_{lm} U_l^{\alpha}(r, E_l) Y_{lm}(\boldsymbol{r}), & r < S_{\alpha} \end{cases} \qquad \text{II-(30)}$$

II.9.4. Linearized augmented plane wave method (LAPW)

Although the PP-PW method is very efficient and useful, but it always remains an approximation, in addition if we need some information near the nucleus like the hyperfine field or the excitations of the lowest levels, then we cannot use the PP-PW method. therefore, we sometimes must carry out a so-called all electron "all of them" calculation. For this we will need another basis on which to project the electronic wave function. There have been several methods proposed, but I am interested in the FP-LAPW method. The basic idea was proposed by Slater. It follows naturally from the fact that the electrons in the inner shells behave like

electrons in single atoms. They can, as a reason, be conveniently described by atomic (orbital) functions. That is why the potential has spherical symmetry, and the wave functions are oscillatory. Far from the nuclei, in the interstitial regions, the electrons are free. They are best described by plane waves.

Thus, space is divided into two regions: atomic spheres of radius Rα centered on each atom, called MT (Muffin-Tin) spheres, and the space between these spheres called interstitial space.[27]

As a result, the electronic wave function will be developed in two different bases according to these two regions, namely:

1. Radial parts and spherical harmonics inside MV spheres

2. Plane waves in the interstitial region. Therefore, it is called the APW augmented plane wave method.

II.9.5. Density Functional Disruption Theory (DFPT):

The DFPT method is a well-established method for the ab initio study of the dynamics of networks of solids [28]. Allows the system responses to be calculated to disturbances λ, it is based on the perturbative extension of the DFT. The linear response provides an analytical way to calculate the second derivative of the total energy with respect to a given disturbance. Depending on the nature of this disturbance, a number of properties can be calculated, for example a disturbance in ionic positions (atomic shift) gives the dynamic matrix and phonons, a disturbance in the magnetic field and the answer is NMR, a disturbance in the unit vectors of the mesh (strain) and the response is the elastic constants, a disturbance in an electric field and the response is dielectric [29].

The DFPT is implemented in the ABINIT code [30] to calculate the dynamic matrix, the frequencies of the phonons, the effective charges, and the elastic constants.

II.10. Used codes

II.10.1. The Wien2k code

Now days such calculations can be done on sufficiently powerful computers for systems containing about 100 atoms per unit cell.

Chapter II: Methods & concepts

In solids, we often start with an ideal crystal that is studied on the atomic scale. Quantum mechanics governs the electronic structure that is responsible for properties. Corresponding first principles calculations are mainly done within (DFT), according to which the many-body problem of interacting electrons and nuclei is mapped to a series of one-electron equations, the so-called (KS) equations. One among the most precise schemes to solve the KS equations is the (LAPW) method that is employed for example in the computer code WIEN2k to study crystal properties on the atomic scale, such as relative stability, chemical bonding, relaxation of the atoms, phase transitions, electrical, mechanical, optical, or magnetic behavior, etc. [31].

II.10.2. The ABINIT code

The mechanical properties in this thesis were carried out using the Abinit code [http://www.abinit.org] [32], is a software allowing to find the total energy, the density of charge and the electronic structure of systems composed of electrons and nuclei (molecules and periodic solids) through the functional theory of DFT density, and linear response (DFPT), using pseudopotentials and a plane wave base. Abinit also includes options to perform molecular dynamics simulations, or to generate dynamic matrix, effective Born charge, and dielectric tensors.

The Abinit program is a first principles program that calculates the properties of molecules and solids. One of the advantages of this code is that it is free software. Abinit is a project distributed under the GNU license (GPL http://www.gnu.org/copyleft/gpl.txt) whereby the sources are and must remain freely accessible to anyone.

Chapter II: Methods & concepts

II.11. References

[1] Heitler, Walter Heinrich. "Erwin Schrödinger, 1887-1961." (1961): 221-228.

[2] Schrödinger, Erwin. "An undulatory theory of the mechanics of atoms and molecules." *Physical review* 28.6 (1926): 1049.

[3] Schrödinger, Erwin. "Quantisierung als eigenwertproblem." *Annalen der physik* 385.13 (1926): 437-490.

[4] Sholl, David, and Janice A. Steckel. *Density functional theory: a practical introduction*. John Wiley & Sons, 2011.

[5] Born, M., et al. "On the Quantum Theory of Molecules." *Ann. Physik* 84 (1927): 457.

[6] D.R. Hartree, Proc. Cambridge Philos. Soc. 24 (1928) 89.

[7] Fock, Vladimir. "Näherungsmethode zur Lösung des quantenmechanischen Mehrkörperproblems." *Zeitschrift für Physik* 61.1-2 (1930): 126-148.

[8] P. Hohenberg and W. Kohn, Physical Review 136(3B) (1964) p. 864 version 2.00, created on August 7, 2013.

[9] Thomas, Llewellyn H. "The calculation of atomic fields." *Mathematical proceedings of the Cambridge philosophical society*. Vol. 23. No. 5. Cambridge University Press, 1927.

[10] Fermi, Enrico. "Eine statistische Methode zur Bestimmung einiger Eigenschaften des Atoms und ihre Anwendung auf die Theorie des periodischen Systems der Elemente." *Zeitschrift für Physik* 48.1-2 (1928): 73-79.

[11] W. Kohn and L. J. Sham, "Self-Consistent Equations Including Exchange and Correlation Effects," Phys. Rev., vol. 140, no. 4A, pp. A1133–A1138, Nov. 1965.

[12] P. Hohenberg and W. Kohn, "Inhomogeneous Electron Gas," Phys. Rev., vol. 136, no. 3B, pp. B864–B871, Nov. 1964.

[13] R. M. Martin, Electronic structure: basic theory and practical methods. Cambridge University Press, 2004.

[14] Perdew, John P., and Alex Zunger. "Self-interaction correction to density-functional approximations for many-electron systems." *Physical Review B* 23.10 (1981): 5048.

[15] Ceperley, D. M., and B. J. Alder. "Accurate and simple analytic representation of the electron-gas correlation." Phys. Rev. Lett 45 (1980): 566-569.

[16] J. P. Perdew, K. Burke, and M. Ernzerhof, "Generalized Gradient Approximation Made Simple," Phys. Rev. Lett., vol. 77, no. 18, pp. 3865–3868, Oct. 1996.

[17] Wang, Lei, Thomas Maxisch, and Gerbrand Ceder. "Oxidation energies of transition metal oxides within the GGA+ U framework." *Physical Review B* 73.19 (2006): 195107.

[18] J. P. Perdew and Y. Wang, "Accurate and simple analytic representation of the electron-gas correlation energy," Phys. Rev. B, vol. 45, no. 23, pp. 13244– 13249, Jun. 1992.

[19] Langreth, David C., and M. J. Mehl. "Beyond the local-density approximation in calculations of ground-state electronic properties." *Physical Review B* 28.4 (1983): 1809.

[20] Tancogne-Dejean, Nicolas, and Angel Rubio. "Parameter-free hybridlike functional based on an extended Hubbard model: DFT+ U+ V." *Physical Review B* 102.15 (2020): 155117.

[21] Wang, Lei, Thomas Maxisch, and Gerbrand Ceder. "Oxidation energies of transition metal oxides within the GGA+ U framework." *Physical Review B* 73.19 (2006): 195107.

[22]. Dudarev, S. L., et al. "Electron-energy-loss spectra and the structural stability of nickel oxide: An LSDA+ U study." *Physical Review B* 57.3 (1998): 1505.

[23]. Singh, David J., and Lars Nordstrom. *Planewaves, Pseudopotentials, and the LAPW method*. Springer Science & Business Media, 2006.

[24] S. L. Dudarev, G. A. Botton, S. Y. Savrasov, C. J. Humphreys, and A. P. Sutton, Phys. Rev, B 57 (1998) 1505.

[25] Austin, B. J., V. Heine, and L. J. Sham. "GENERAL THEORY OF PSEUDOPOTENTIALS." *Physical Review (US) Superseded in part by Phys. Rev. A, Phys. Rev. B: Solid State, Phys. Rev. C, and Phys. Rev. D* 127 (1962).

[26] Cottenier, Stefaan. "Density Functional Theory and the family of (L) APW-methods: a step-by-step introduction." *Instituut voor Kern-en Stralingsfysica, KU Leuven, Belgium* 4.0 (2002): 41.

[27] Andersen, O. Krogh. "Linear methods in band theory." *Physical Review B* 12.8 (1975): 3060.

[28] Blaha, Peter, et al. "wien2k." *An augmented plane wave+ local orbitals program for calculating crystal properties* 60 (2001).

[29] Baroni, Stefano, et al. "Phonons and related crystal properties from density-functional perturbation theory." *Reviews of modern Physics* 73.2 (2001): 515.

[30] http://www.sers.york.ac.uk/~mijp1/teaching/grad-FPMM/practical-classes/MS- CASTEP - guid.

[31] Hellmann, H. "Einfuhrung in die Quantenchemie (Deuieke, Leipzig); Feynman RP 1939." *Phys. Rev* 56 (1937): 340

[32] Pouillon, Y. *What is Abinit*. 2014 2014/06/02; Available from: https://wiki.abinit.org/doku.php#dokuwiki_top.

Books For reading

- Eschrig, Helmut. *The fundamentals of density functional theory*. Vol. 32. Stuttgart: Teubner, 1996.
- Giustino, Feliciano. *Materials modelling using density functional theory: properties and predictions*. Oxford University Press, 2014.
- Sholl, David, and Janice A. Steckel. *Density functional theory: a practical introduction*. John Wiley & Sons, 2011.

"If it scares you, it might be a good thing to try."

-Seth Godin

Chapter III: Results and discussion

Chapter III: Results and discussion

III.1 Introduction

In this work, we pay attention to the structural**,** electronic, and magnetic properties of ternary antiperovskite compounds: Mn_3ZnC, Mn_3GaC, and Mn_3GaN which are investigated using first principles calculations based on FP-LAPW method implemented in Wien2k code. Parallelly their mechanical properties also are examined by DFPT method implemented in ABINIT code.

III.2. Partie (1): Properties calculations by Wien2k code

III.2.1. Calculation details

All the structural, electronic, and magnetic properties of carbides and nitrides antiperovskites, were performed with density functional theory (DFT) by using the full potential linear augmented plane wave (FP-LAPW) [1] method as implemented in Wien2k package [2]. For the exchange-correlation energy, we used the generalized gradient approximation (GGA) proposed by Wu–Cohen (WC-GGA) [3].

The strongly correlated electron systems with localized d orbitals are usually not defined well in accuracy by GGA functional. In such a case, the on-site Coulomb interaction with an effective Hubbard U parameter (GGA+U) is included using the approach of Dudarev et al[4]. The Hubbard potential use as a prototype for the strongly correlated orbitals (in many of materials mentioned above, these orbitals are actually d orbitals [5]. In GGA+U approach, we treated 3d electrons of Mn as valence electrons by selecting those value of U parameter (U=3.5 eV) [6].

The separation energy between the core and valence states is kept at − 6.0 Ry. The wave functions inside the atomic spheres in the full potential scheme for these materials are expanded in terms of spherical harmonics up to $l_{max} = 10$.

In order to achieve energy and charge convergence, the $R_{MT} \times K_{MAX}$value was set to 7 (R_{MT} refers to the small atomic radius in the unit cell, while K_{max} is the size of the largest vector in the plane wave expansion), and k sampling with 120 k-points in the irreducible part of the Brillouin zone ($15 \times 15 \times 15\ k - mesh$) were used. The plane waves cut off value for the charge density and potential is selected to be $G_{MAX} = 12\ (Ry)^{1/2}$. The atomic muffin-tin radius (R_{MT}) spheres and valence states used for these materials are presented in Table III.1:

Table III. 1: Properties and applications of some antiperovskites materials.

Compound	Crystal . P/S.G	Functional	Electronic Configuration	R_{MT} (Bhor)	$R.K_{Max}$	$K-Point$
Mn_3ZnC	Cubic (Pm-3m n°221)	WC-GGA	[Mn]:[Ar] $3d^5 4s^2$ [Zn]:[Ar] $3d^{10}4s^2$ [C]:[He] $2s^2 2p^2$	Mn:1.9 Zn:2.5 C:1.5	7	$15 \times 15 \times 15$ 120
Mn_3GaC			[Mn]:[Ar] $3d^5 4s^2$ [Ga]:[Ar] $3d^{10}4s^2 4p^1$ [C]:[He] $2s^2 2p^2$	Mn:1.9 Ga:2.5 C:1.5		
Mn_3GaN			[Mn]:[Ar] $3d^5 4s^2$ [Ga]:[Ar] $3d^{10}4s^2 4p^1$ [N]:[He] $2s^2 2p^3$	Mn:1.75 Ga:2.5 N:1.5		

III.2.2. Crystallographic structure

The geometries structure of carbides and nitrides antiperovskites $Mn_3AX, A(Zn, Ga), X(C, N)$ illustrated in figure (III.1), exhibit a cubic structure with the space group $Pm\bar{3}m$ (n°221). This structure consisting of Zn and Ga atoms at the corners $(0, 0, 0)$, $C\ and\ N\ atoms$ at the body centre$(0.5, 0.5, 0.5)$, and Mn atoms at the face centres of the cube $(0.5, 0.5, 0)$. In this work we studied three phases: non-magnetic (NM), ferromagnetic (FM), and antiferromagnetic (AFM), The magnetic structure of the AFM phase is obtained by constructing a supercell of $1 \times 1 \times 2$ which contains two cubic cells wherein the magnetic sub-lattice (anion sub-lattice), the AFM order is along the z-axis as schematically represented in figure III.1.

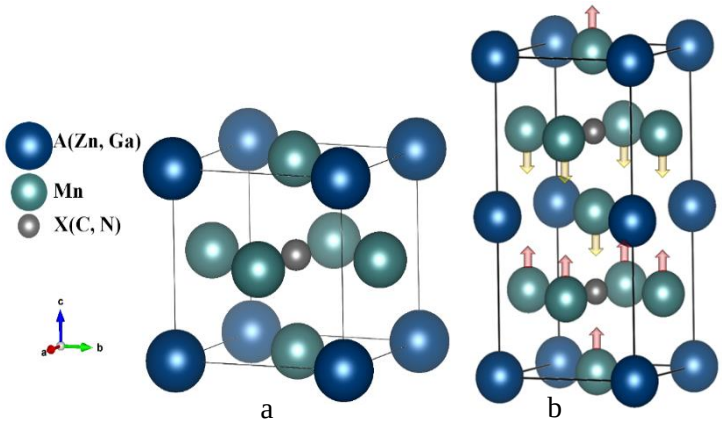

Figure III. 1: (a) Crystallography structure of Mn_3AX, (b) Unit cell of the AFM configuration

Chapter III: Results and discussion

III.2.3 Structural properties and magnetic ordering

The total energy was calculated as a function of volume to determine, at equilibrium, the structural properties such as the lattice constant and the compressibility module B and its derivative at P = 0 GPa and T = 0 K. The optimization is carried out by calculating the total energy according to volume using GGA and GGA+U approximations. Experimental lattice constants [7], [8], [9], for ($Mn_3ZnC - Mn_3GaC - Mn_3GaN$) respectively, are used as input for the structural optimization.

In order to study the magnetic ordering, we compare the total energy of carbides and nitrides antiperovskites ($Mn_3ZnC - Mn_3GaC - Mn_3GaN$) in different magnetic phases: non-magnetic (NM), ferromagnetic (FM), and antiferromagnetic (AFM) phases, the results are represented in figure III.2.

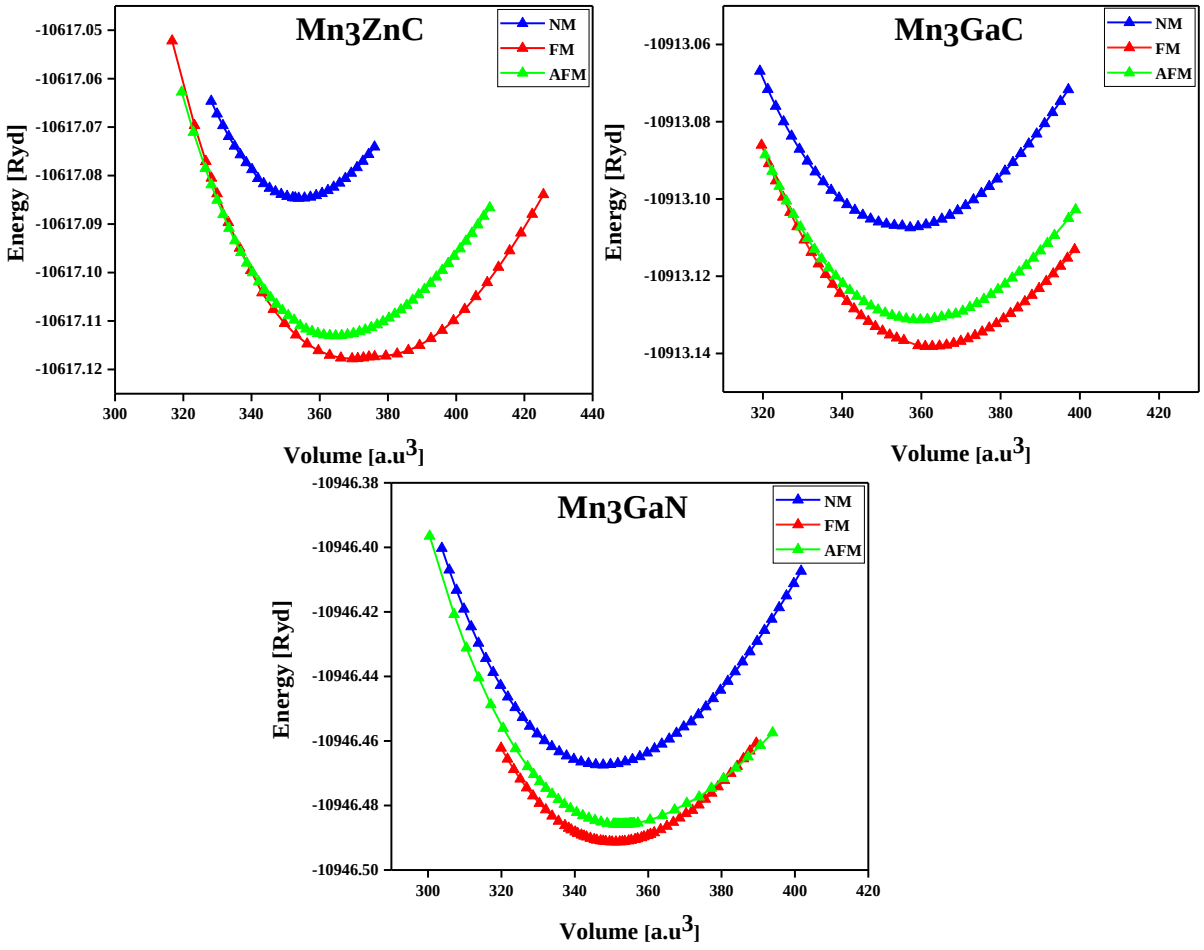

Figure III. 2: Total energy as a function of formula unit volume for 3 compounds for FM, NM, and AFM phases by WC-GGA functional.

As can be seen from this figure for three compounds the ferromagnetic state is the most stable phase due to their lowest energy in comparison with cases of NM and AFM ordering.

Moreover, for Mn_3ZnC, Mn_3GaC, and Mn_3GaN compounds, we remark there is second order phases transitions from AFM to FM phase, depending on the Birch-Murnaghan equation of state [10] we calculate the pressures, and we found his values P=19.87 GPa, P=39.20 GPa, and P= -18.55 GPa for Mn_3ZnC, Mn_3GaC, and Mn_3GaN compounds, respectively.

Figure III.3 shows the optimization of the total energy according to volume for three compounds in FM phase using GGA+U potential.

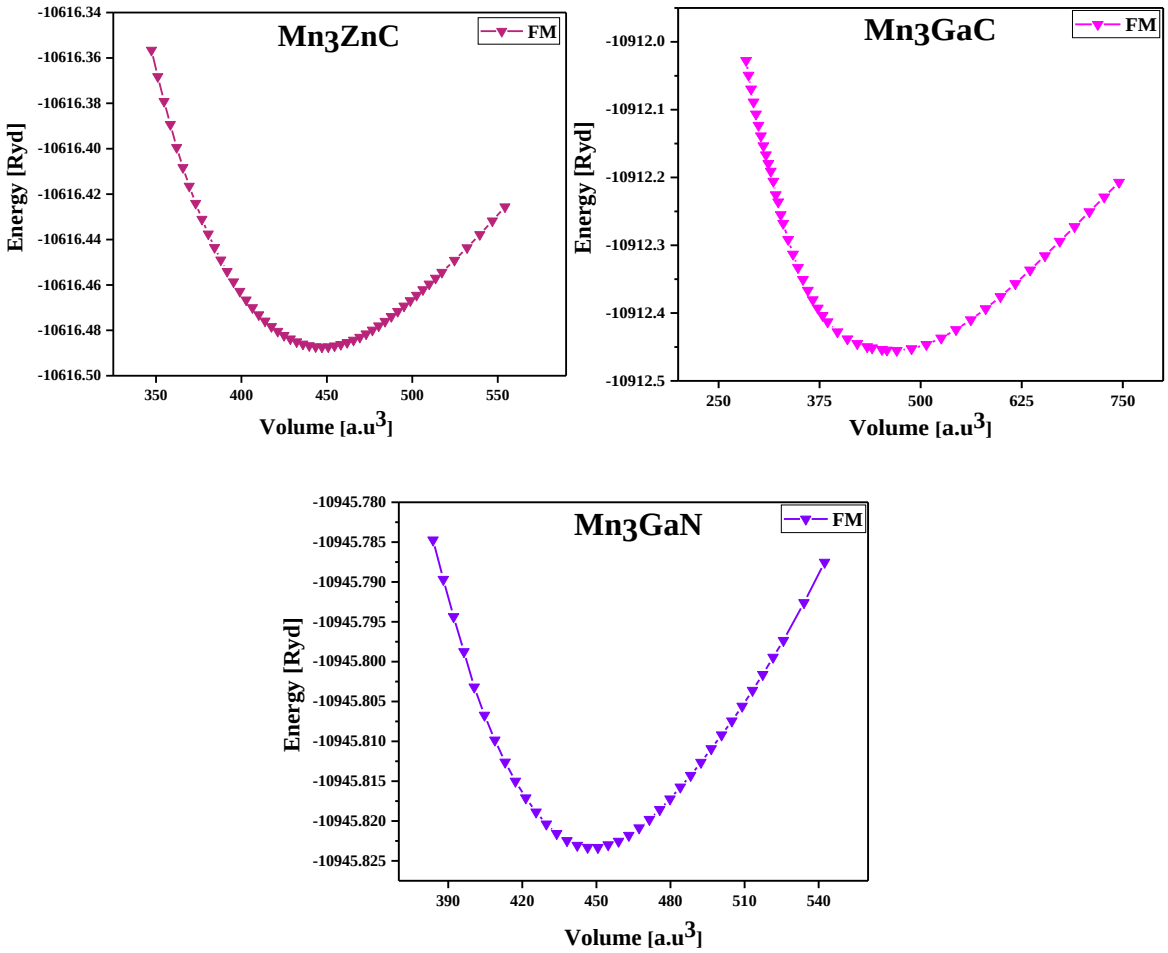

Figure III. 3: Total energy as a function of formula unit volume for 3 compounds for FM phase by GGA+U potential.

In addition, from fitting this data to Birch-Murnaghan equation of state, and along the hydrostatic path, the equilibrium lattice parameter, bulk modulus, and its derivative, as shown

in Table III.2, are obtained for each phase. For comparison, Experimental values and those obtained by other calculations are also given in (Table III.2).

Table III. 2: Calculated lattice parameter (Å), bulk modulus (GPa), its derivative pressure, and ground state energy (Ry) for (Mn_3ZnC-Mn_3GaC-Mn_3GaN) in its FM, NM, and AFM phases.

Compound	Fun	Phase	$a\ (A°)$	$B(GPa)$	B'	Other work	Exp	$\frac{\Delta a}{a}$%	r(A°)
Mn_3ZnC	WC-GGA	NM	3.74	264.73	4.36	3.81[11] 3.86[12]	3.9164[7] T(400°K)	3.22	r_{Zn}=0.74 r_{Ga}=0.62 r_C=0.16 r_N=0.13
		FM	**3.79**	**168.79**	**5.11**				
		AFM	3.78	187.96	6.09				
	GGA+U	FM	4.04	107.22	4.78			3.15	
Mn_3GaC	WC-GGA	NM	3.75	262.95	4.39	3.77[11]	3.896[8] T(293°K)	3.29	
		FM	**3.76**	**241.14**	**4.30**				
		AFM	3.76	238.21	4.72				
	GGA+U	FM	4.11	91.37	3.72			3.95	
Mn_3GaN	WC-GGA	NM	3.72	275.77	4.53	-	3.898[9] T(273°K)	4.22	
		FM	**3.73**	**260.56**	**5.03**				
		AFM	3.73	230.32	6.07				
	GGA+U	FM	4.06	84.40	6.32			4.15	

As shown in the table III.2, we can easily observe for the three compounds that our calculated equilibrium lattice constant (a), For Mn_3ZnC (3.79 Å using GGA and 4.04 Å using GGA+U), Mn_3GaC (3.76 Å using GGA and 4.11 Å using GGA+U), and Mn_3GaN (3.73 Å using GGA and 4.06 Å using GGA+U), are close to the experimental data (3.9164, 3.896, 3.898) respectively. In addition, the use of the GGA slightly underestimates the lattice constant compared to the GGA+U approximation, which thus yields theoretical results in good agreement with experimental reports. However, the calculated lattice constants are underestimated about 3.22%, 3.29% and 4.22% for Mn_3ZnC, Mn_3GaC and Mn_3GaN, respectively with WC-GGA functional, and 3.15%, 3.95%, and 4.15 for Mn_3ZnC, Mn_3GaC and Mn_3GaN, respectively with GGA+U potential.

Based on our results of WC-GGA functional, lattice constant increases as A atoms goes in the order $Ga \rightarrow Zn$ and X atoms goes in the order $N \rightarrow C$ due to the increase of atomic size in this direction.

Chapter III: Results and discussion

The bulk modulus B, its pressure derivative B' and the computed values for ($Mn_3ZnC - Mn_3GaC - Mn_3GaN$) are listed in table II.3. The computed values of bulk modulus for these compounds with GGA functional are 168.63 GPa, 241.14 GPa and 260.56 GPa, respectively, which shows that on changing the cations (Zn-Ga), the incompressibility of the material increases, and hence, the material become more compressible.

Great consistence is observed between our calculations within the GGA method for the geometry of Mn-based APVs is in good agreement with experimental results and others.

III.2.4 Magnetic properties

The optimized structure in the ferromagnetic configuration was adopted to determine the spin magnetic moment for these compounds $Mn_3ZnC - Mn_3GaC - Mn_3GaN$, using the formalism of the generalized gradient approximation WC-GGA and GGA + U potential, who was performed in our calculation as a comparison. On the other hand, relativistic effects are also included in the calculation by considering the spin orbit coupling (SO). The magnetic moment of these compounds results from the sum of the partial moments of the different elements (Zn, Ga, Mn, C and N) and the moment of the interstitial zone.

Table (III.3) reports the calculated local and total magnetic moments in interstitial and spherical region for the studied Mn-based antiperovskites.

For WC-GGA functional, the total magnetic moments are $5.81\mu_B$, $3.83\mu_B$ and $2.69\mu_B$ for Mn_3ZnC , Mn_3GaC and Mn_3GaN, respectively, and very small values of local magnetic moments for the Zn, Ga, C, N atoms. One can note that the magnetism of the considered antiperovskites comes mainly from the transition metal Mn with atomic magnetic moment of $1.77\mu_B$ in Mn_3ZnC, $1.24\mu_B$ in, Mn_3GaC and $0.85\mu_B$ in Mn_3GaN.

After we applied the Hubbard potential, we observed an increasing in the total magnetic moments from 5.81 to 10.98 for Mn_3ZnC, from 3.83 to 11.68 for Mn_3GaC, and from 2.69 to 11.34 for Mn_3GaN. The magnetic moments of Mn are $3.57\mu_B$, $3.54\mu_B$, and $3.43\mu_B$ for Mn_3ZnC , Mn_3GaC and Mn_3GaN, respectively. However, our values of Mn moment are consistent with those of $\mu_{Mn} = 3 - 4\,\mu_B$ observed in many manganese intermetallic compounds.

Then we applied spin orbit coupling, we remark a decreasing in the local and total magnetic moments, return to the initial values it is means that the spin orbit coupling cancelled the effect of Hubbard potential.

Table III. 3: The local and total magnetic moment for (Mn_3ZnC-Mn_3GaC-Mn_3GaN).

Compound		Functional	$m_{interstitial}$	m_{Mn}	m_A	m_C	m_{tot}
$\mathbf{Mn_3ZnC}$	Our calcul	WC-GGA	0.40	1.77	-0.04	-0.11	5.81
		GGA+U	**0.73**	**3.57**	**-0.25**	**-0.22**	**10.98**
		GGA+U+SO	0.40	1.76	-0.04	-0.11	5.54
	Other work[12,13]	PBE-GGA	0.15	2.37	-0.009	-0.16	7.01
		PW91-GGA	-	2.62	-0.46	-0.38	7.02
$\mathbf{Mn_3GaC}$	Our calcul	WC-GGA	0.26	1.24	-0.07	-0.08	3.83
		GGA+U	**1.39**	**3.54**	**-0.20**	**-0.14**	**11.68**
		GGA+U+SO	0.26	1.24	-0.07	-0.08	3.82
$\mathbf{Mn_3GaN}$	Our calcul	WC-GGA	0.26	0.85	-0.07	-0.06	2.69
		GGA+U	**1.26**	**3.43**	**-0.16**	**-0.06**	**11.34**
		GGA+U+SO	0.26	0.85	-0.07	-0.06	2.69

III.2.5 Electronic properties

The band structure (BS) and the density of states (DOS) are the dominant quantities that determine the electronic structure of a system. Their inspection provides information about the electronic properties (metal, insulator, or semiconductor) and gives insight into the chemical bonding. Since the equilibrium ground state was found, we have calculated the band structure and the total densities of states at the ferromagnetic state.

III.2.5.1 Band structure

In order to understand the concepts of the band structure it is convenient to introduce the concept of k-points here. There are an infinite number of k-points in the Brillouin zone.

Band structure calculations performed on crystalline solids require the evaluation of integrals over the Brillouin zone, that cannot be performed analytically. This problem is overcome by the fact that k-points that are sufficiently close together contain similar information; we can therefore replace the integration with a summation over a finite number of k-points. The number of points required to obtain converged properties will depend on the size and nature of the system. For example, metallic systems tend to require more k-points (to capture the shape of the Fermi surface properly) than a large band-gap insulator. A common recipe for choosing the number of k-points was that developed by Monkhorst and Pack[14], which is particularly well suited for metallic systems, but is applied more generally to all crystalline solids [15].

Chapter III: Results and discussion

The Figure (III.4) show the Brillouin zone related to the simple cubic structure, with k-points of high symmetry, used in calculations of band structure carried out in the present study. The four points k of high symmetry of the ZB for the cubic network have the following coordinates: Γ(0 0 0), R (0.5 0.5 0.5), M (0.5 0.5 0) and X (0.5 0 0) [16].

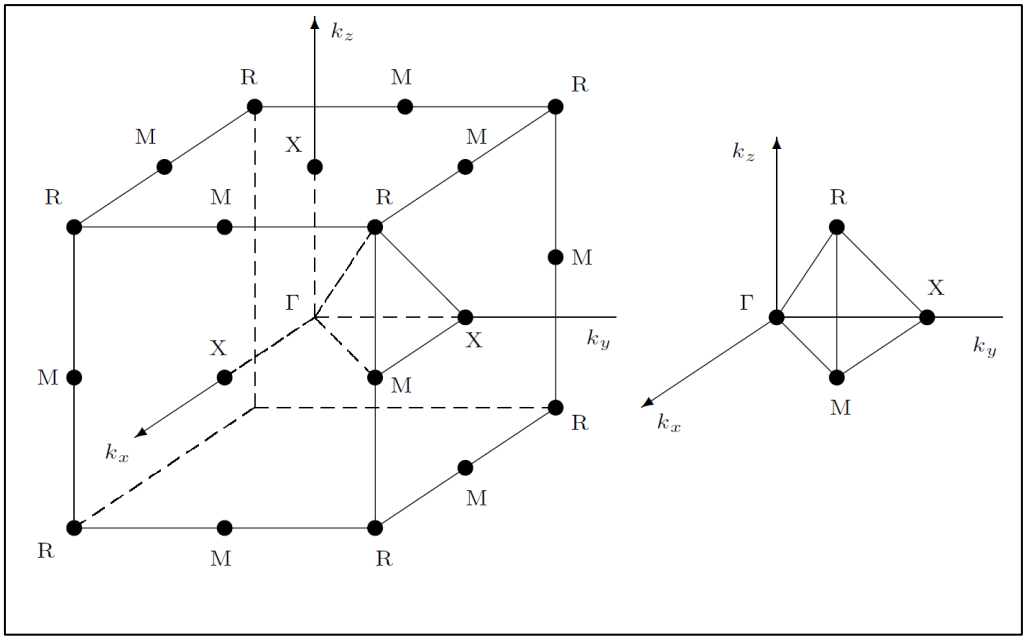

Figure III. 4: The first Brillouin zone of the cubic, space group (Pm-3m n°221)

At the equilibrium lattice constants of Mn_3AX compounds in FM state, the band structures, for both spin channels (up, and down), is calculated along direction $\Gamma - X - M - \Gamma - R - X$ in the energy range from -8 eV to 8 eV. The comparative band structure for Mn_3AX compounds along the high symmetry directions in the Brillouin zone, are shown in figure (III.5) For three compounds, we can clearly see for the two approximations WC-GGA and GGA+U that the valence and conduction bands overlap significantly and there is no band gap at the Fermi level, which allows us to classify them as an electrical conductor.

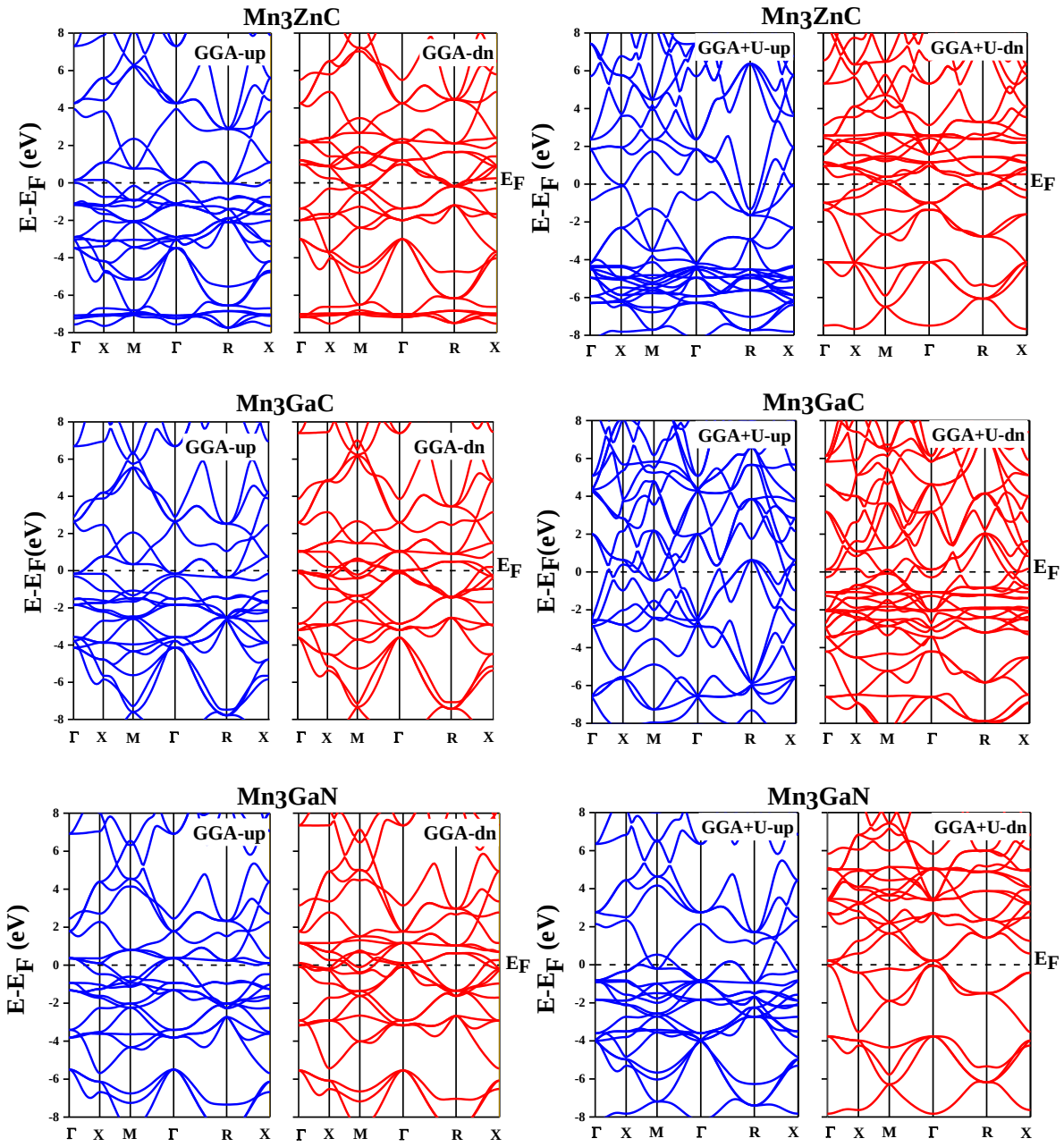

Figure III. 5: Band structure of carbides and nitrides antiperovskites Mn_3AX with GGA and GGA+U potential.

III.2.5.2 Densities of states

The density of states (DOS) of a solid is of fundamental importance in determining its electronic properties. The total and partial density of states (TDOS and PDOS) of Mn-based antiperovskites using GGA and GGA+U are calculated and presented in the next figures.

The majority-spin and minority spin are shown above and below the axes. The TDOS show no energy gap at the Fermi level, indicating the metallic nature of these three compounds. For three compounds, the number of electrons at the Fermi level comes mainly from the spin up and spin-down states of the Mn-3d. The Mn-d electrons are mainly contributing to the DOS at the Fermi level and should be involved in the conduction properties. Carbon, Nitrogen, zinc, and Gallium electrons do not contribute significantly at the Fermi level.

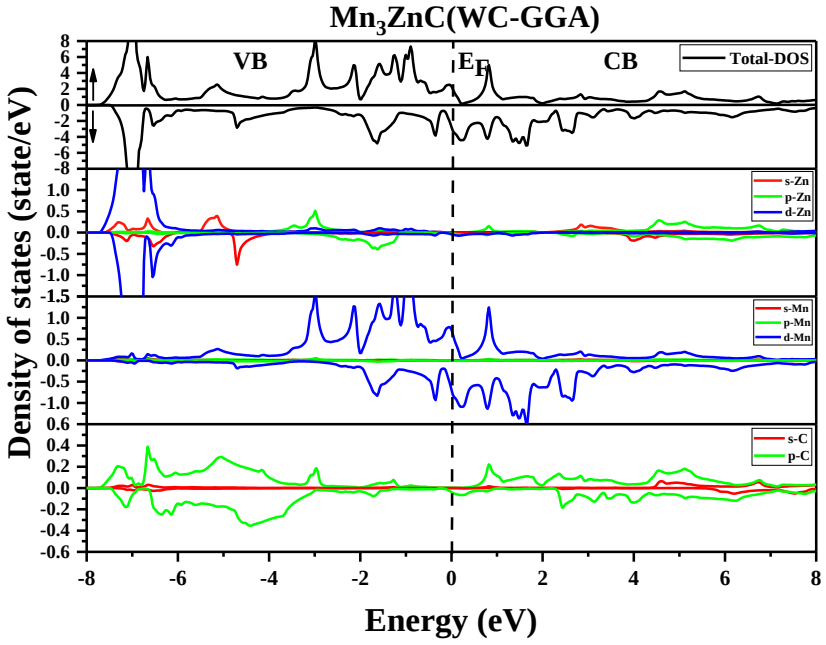

Figure III. 6: Total and partial densities of states for Mn_3ZnC compound with GGA functional.

- ✓ For Mn_3ZnC compound as shown in figure (III.6)

The valence bond devised into three regions:

VB_1: [-8, -6 eV]: The structure is from the Zn-d and C-p states with a small contribution arising from Mn-d.

VB_2: [-6, -4 eV]: This region contains from the Zn-s and C-p states and with small contribution arising from Mn-d.

VB_3: [-3, 0 eV]: If we abandon the Zn-d and C-p states towards the Fermi level, we find Mn-d and Zn-p.

The conduction bond devised into two regions:

CB_1: [0, 4 eV**]:** Contains from the Mn-d and C-p states.

CB_2: [4, 8 eV**]:** Contains from the Mn-d and C-p and Zn-p states.

- ✓ For Mn_3GaC compound illustrated in figure (III.7)

The valence bond devised into two regions:

VB_1: [-8, -4 eV]: The structure located in this region is due mainly to the Ga-s and C-p states with a small contribution arising from Mn-d.

VB_2: [-4, 0 eV]: This region contains from the Ga-p and Mn-d states and with small contribution arising from C-p. The 3d orbitals of Mn have high density of states at Fermi level(E_F).

The conduction bond devised into two regions:

CB_1: [0, 4 eV**]:** Contains from the Mn-d and C-p states with a small contribution arising from Ga-s.

CB_2: [4, 8 eV**]:** Contains from the Ga-p and C-p with a small contribution arising from Mn-d.

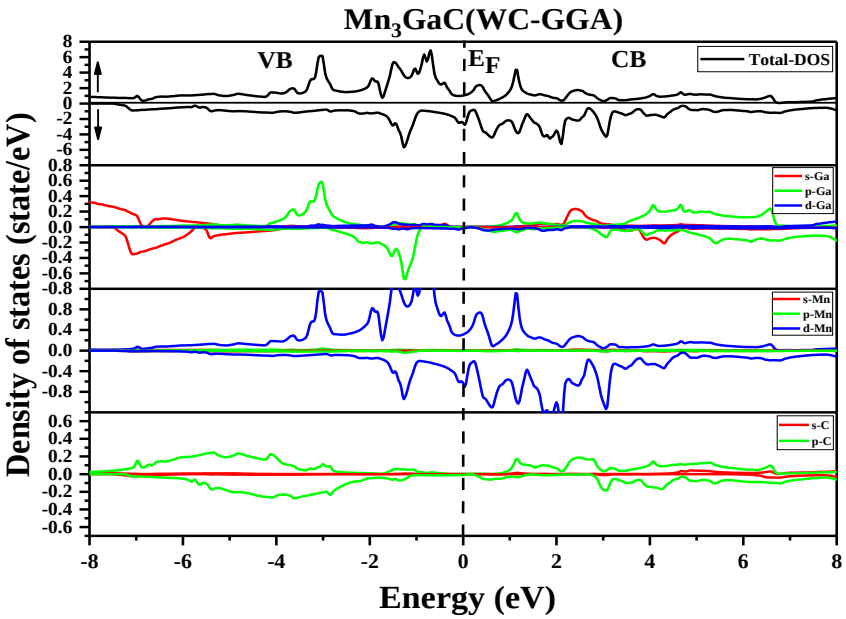

Figure III. 7: Total and partial densities of states for Mn_3GaC compound with GGA functional.

✓ For Mn_3GaN compound as presented in figure (III.8)

The valence bond devised into two regions:

VB_1: [-8, -4 eV]: The structure located in this region is due mainly to the Ga-s and N-p states with a small contribution arising from Mn-d.

VB_2: [-4, 0 eV]: This region contains from the Ga-p and Mn-d states and with small contribution arising from N-p. The 3d orbitals of Mn have high density of states at Fermi level(E_F).

The conduction bond devised into two regions:

CB_1: [0, 4 eV**]:** Contains from the Mn-d and N-p states with a small contribution arising from Ga-s.

CB_2: [4, 8 eV**]:** Contains from the Ga-p and N-p with a small contribution arising from Mn-d.

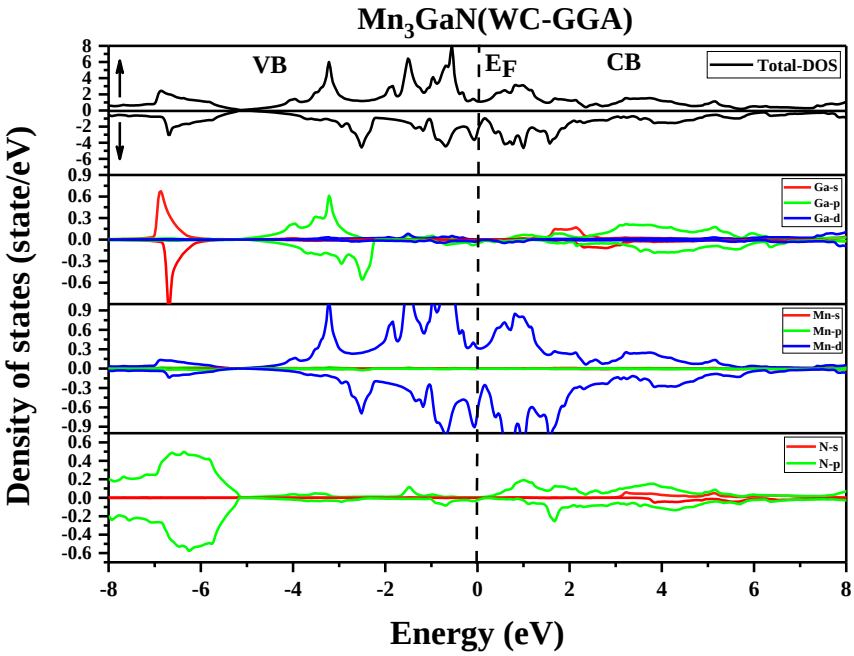

Figure III. 8: Total and partial densities of states for Mn_3GaN compound with GGA functional

The total and partial density of states (TDOS and PDOS) of Mn-based antiperovskites using GGA+U potential are illustrated in figures (III.9- III.10- III.11) coming later.

The metallic character of the compound does not change using GGA+U, however, the shape of the curves varies slightly with a delocalization of some peaks present in the DOS using GGA. Additionally, the asymmetrical nature of spin-up and spin-down graphs from the density of states demonstrate the magnetic nature of these three compounds.

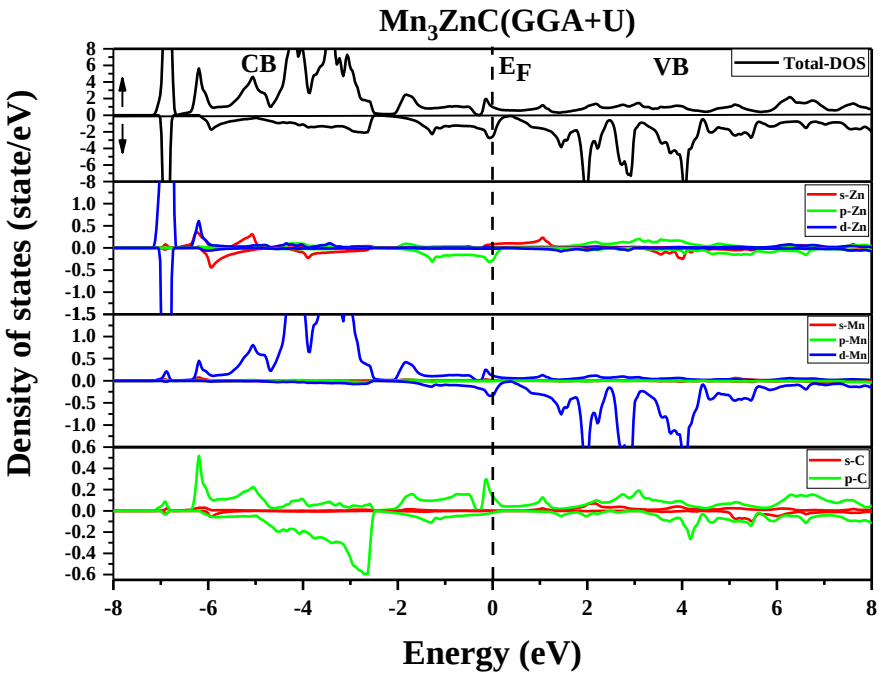

Figure III. 9: Total and partial densities of states for Mn_3ZnC compound with GGA+U potential.

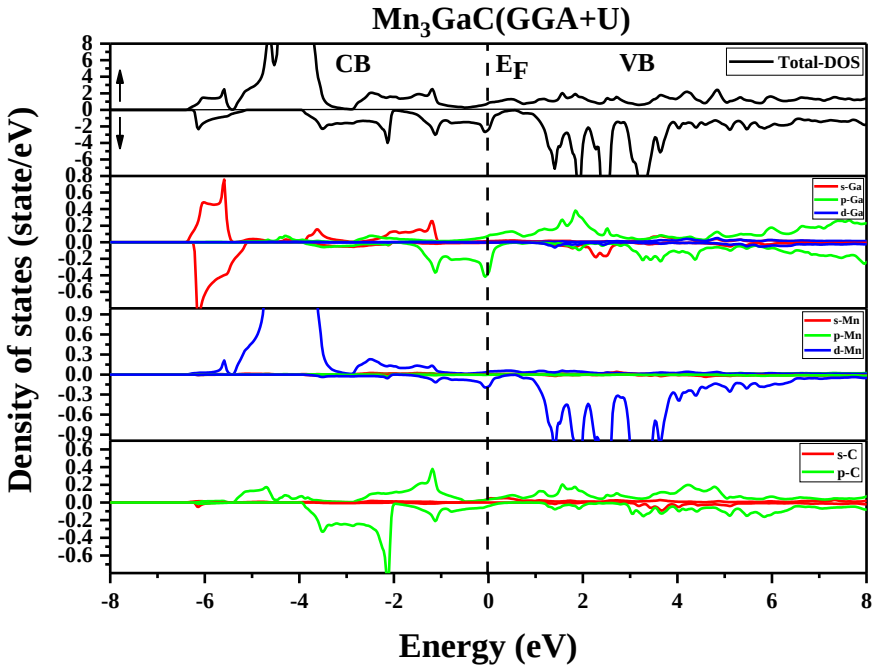

Figure III. 10: Total and partial densities of states for Mn_3GaC compound with GGA+U potential.

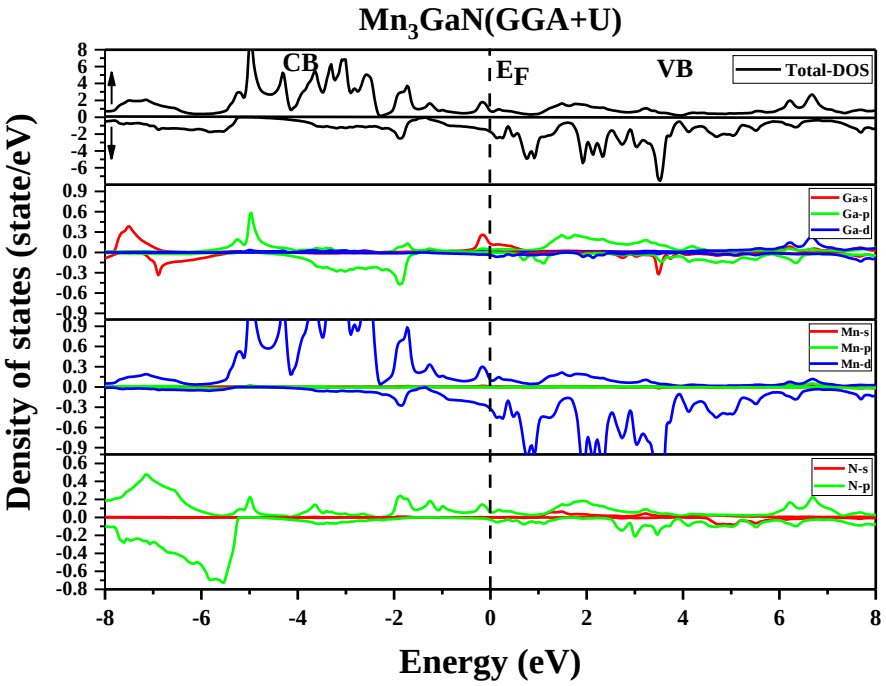

Figure III. 11: Total and partial densities of states for Mn_3GaN compound with GGA+U potential.

III.2.5.3 Electronic charge density

Charge density can provide important information on chemical bonding of materials.

In this work, we have calculated the charge density as illustrated in (Fig II.5.3). From the figure, it is seen clearly that for all three materials, covalent nature is predominant in Mn-C bonding as there is high charge density between Mn and C atoms which is result of the hybridization between Mn-3d and C-2p orbitals. While the charge density in the space between Mn and X atoms is very small, the Mn-X chemical bonding can be attributed to be metallic, that it is generated from the attractive interaction between delocalized conduction electrons (free electrons) in Mn atom and positively charged metal X. Eventually they all lead us to the crystal stability.

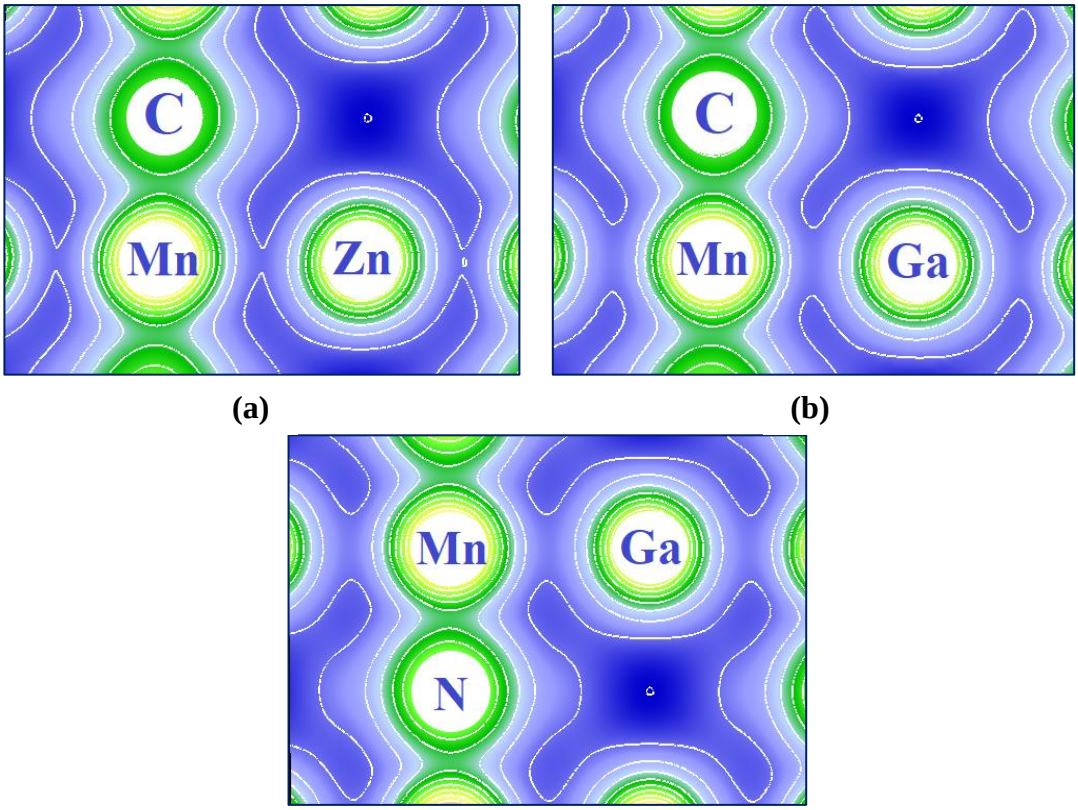

Figure III. 12: Calculated spin-polarized electronic charge density contours for three compounds, (a): Mn_3ZnC, (b): Mn_3GaC, (c): Mn_3GaN

III.2.6 Effect of pressure in magnetic moment

Usually, to induce some significant change in the structures, high pressures are needed for the study of materials. We performed FP-LAPW calculations on the Mn-based antiperovskites to identify the magnetic moment of Mn atom using the GGA approximation, and I applied increasing pressure on my three compounds and examined the corresponding magnetic moment for each compound.

Magnetic moment per Mn as a function of pressure for three compounds depicted in figure (III.13) as we can remark from this figure, the three compounds have linear trend, where the magnetic moment of Mn decreasing with increasing of pressure from zero to 20 GPa for Mn_3ZnC, Mn_3GaN compounds and from Zero to 40 GPa for Mn_3GaC compound.

we conclude that the Mn moment in the FM state may contract due to the large spin fluctuations, which are suppressed by the applications of high pressure. These results indicate that the Mn atoms, and therefore the $Mn_3ZnC - Mn_3GaC - Mn_3GaN$ compounds, under high

applied pressure present good magnetic reactivity with a great potential, which makes it a candidate for magneto-mechanical applications.

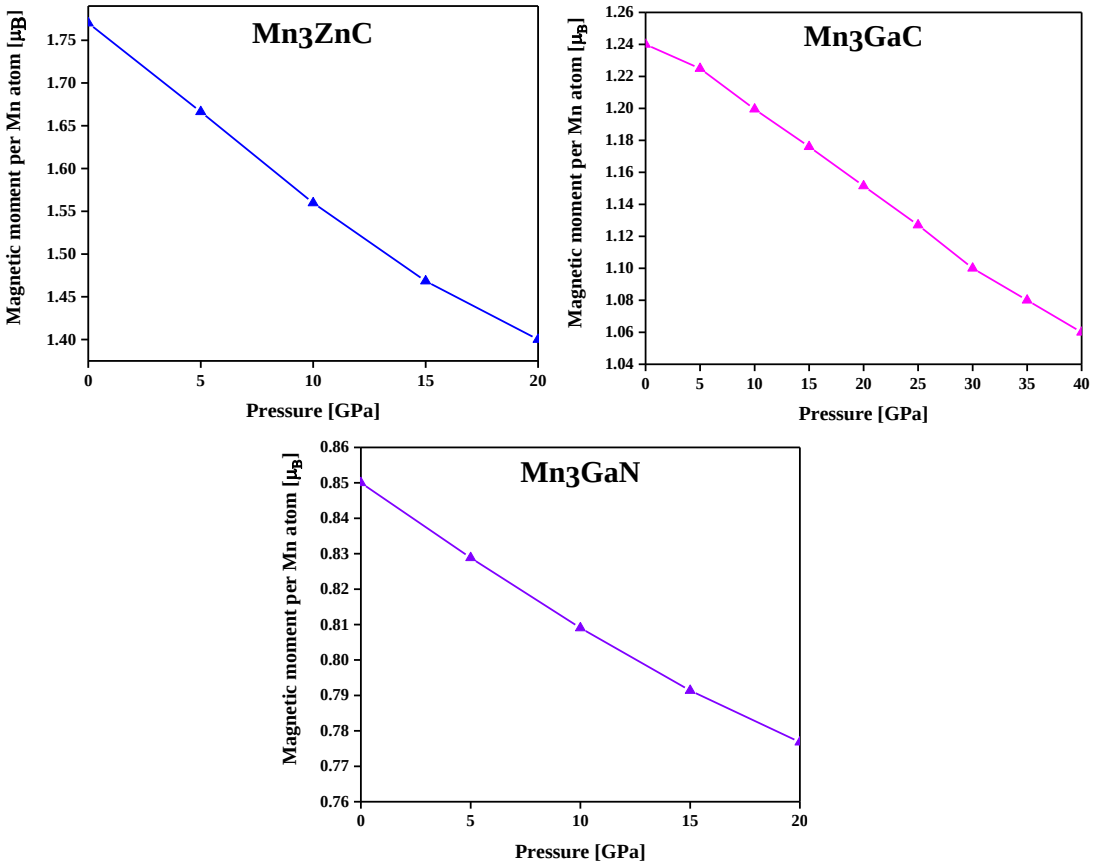

Figure III. 13: Variation of the computed magnetic moment per Mn atom with pressure for three compounds.

III.3. Partie (2): Properties calculations by ABINIT code

In order to explore the structural and elastic properties of the $Mn_3ZnC - Mn_3GaC - Mn_3GaN$ compounds, we used an abinitio calculation method, All these calculations were carried out with the open source software ABINIT [17], developed at the Catholic University of Louvain-la-Neuve, which is a DFT code using the formalism of pseudopotentials for the description of core electrons.

III.3.1 Structural properties

To calculate the lattice constants at thermodynamic equilibrium, we used the structural optimization method based on the minimization technique of Broyden-Fletcher-Goldfarb-Shanno (BFGS) [18], with experimental structures as a starting point, to be able to compare

with the literature and to better understand this structure. Then we relaxed our compounds (changes in the sizes of lattice constant respecting the Hellmann Feynman force minimization principle which uses the algorithm of the conjugate gradient and atomic position shifts). From of the optimized structure, we can calculate the different properties (electronic, elastic, and vibrational…etc).

The lattice constants obtained of the three compounds are reported in Table (III.4) respectively with the experimental values.

Table III. 4: The results of structural optimization of Mn-based antiperovskites compounds.

Compound	a ($A°$)	a_{Exp} ($A°$)	$(\frac{\Delta a}{a}\%)$
Mn_3ZnC	3.71	3.91[7]	5.11
Mn_3GaC	3.70	3.896[8]	5.03
Mn_3GaN	3.69	3.898[9]	5.59

As we can see in this table, there is consistence between our calculations of the Mn-based APVs and experimental results. However, the calculated lattice constants are underestimated about 5.11%, 5.03% and 5.59% for Mn_3ZnC, Mn_3GaC and Mn_3GaN, respectively.

III.3.2 Elastic constants and related properties

Elastic constants are important parameters of material investigated which can provide a link between the mechanical and dynamical stability. It is the physical quantity that describes the elasticity of the material and its response of the crystal to the external forces. An elastic property is the measurement of the tendency of a solid to deform non-permanently in various directions when stress is applied.

Using elastic constants, we can also describe the mechanical stability and bonding nature of the crystals and give important information about the fundamental properties of the solid state such as: the equation of states, the spectra of the phonons and they are related thermodynamically at specific heat, thermal expansion, temperature of Debye, the melting point and the Gruneissen parameter, nature of the forces and bonding.

III.3. 2. 1 Elastic constants

independent elastic constants are determined using the DFPT implemented in ABINIT, for the cubic crystal, there are only three independent elastic constants: C_{11}, C_{12} and C_{44}. The elastic

constant C_{11} reflects the resistance of the crystal to unidirectional compression in the main directions, i.e, the resistance to stress (compression or traction) applies on the planes {100} following the directions <100>. The constant C_{44} represents the shear stress resistance applied to the plane (100) in the direction [010]. The C_{12} constant has no simple physical significance but its combination with other constants provides additional information about the elastic behaviour of cubic materials [16].

For three compounds these constants are distributed in the following tensors:

$$C_{cubique} = \begin{pmatrix} C_{11} & C_{12} & C_{12} & 0 & 0 & 0 \\ C_{12} & C_{11} & C_{12} & 0 & 0 & 0 \\ C_{12} & C_{12} & C_{11} & 0 & 0 & 0 \\ 0 & 0 & 0 & C_{44} & 0 & 0 \\ 0 & 0 & 0 & 0 & C_{44} & 0 \\ 0 & 0 & 0 & 0 & 0 & C_{44} \end{pmatrix} \quad \text{(III-1)}$$

The mechanical stability of a cubic system requires that the three independent elastic constants C_{11}, C_{12} and C_{44} obey the following Born conditions [19]:

$$(C_{11} - C_{12}) > 0\,;\ \ (C_{11} + 2C_{12}) > 0\,;\ \ C_{11} > 0\,;\ C_{44} > 0 \quad \text{(III-2)}$$

and the compression module B must meet the criteria:

$$C_{12} < B < C_{11} \quad \text{(III-3)}$$

Table III. 5: The elastic constants calculated for the three compounds.

Compound		**Elastic constants**		
		$\mathbf{C_{11}}$	$\mathbf{C_{12}}$	$\mathbf{C_{44}}$
$\mathbf{Mn_3ZnC}$	Our work	799.32	182.04	196.78
	Other work[13]	304	40	135
$\mathbf{Mn_3GaC}$	Our work	875.37	196.22	225.70
$\mathbf{Mn_3GaN}$	Our work	707.97	186.40	182.61

It is clearly that the values obtained of elastic constants (C_{ij}) for the three antiperovskites obey the previous conditions, thus indicating the mechanical stability of ($Mn_3ZnC - Mn_3GaC - Mn_3GaN$). We observe that C_{11} is about two and three times higher than C_{12} and C_{44} for the three compounds indicating that they are less compressible along the x -direction.

Chapter III: Results and discussion

The calculation of the elastic constants C_{ij}, allows us to deduce the elastic moduli: Compression, Young's modulus, Shears, as well as Poisson's ratio and anisotropy.

To calculate the moduli of rigidity B and shear G we will use the two approximations of Voigt [20] and Reuss [21] then we take the average between these two approximations (Hill's approximation) [22].

For cubic symmetry we have the formulas which allow us to calculate the shear modulus as well as the rigidity modulus given by the following relations:

$$G_v = \frac{1}{5}(C_{11} + C_{12} + 3C_{44}) \quad \text{(III-4)}$$

$$G_R = \frac{5C_{44}(C_{11}-C_{12})}{4C_{44}+3(C_{11}-C_{12})} \quad \text{(III-5)}$$

Young's modulus and Poisson's ratio are calculated by:

$$E = \frac{9BG}{3B+G} \quad \text{(III-6)}$$

$$\nu = \frac{3B+2G}{2(3B+G)} \quad \text{(III-7)}$$

With $$G = \frac{1}{2}(G_v + G_R) \quad \text{(III-8)}$$

The computed parameters like Bulk modulus (B), Shear modulus (G), Young's modulus (E), Poisson's ratios (σ), of $Mn_3ZnC - Mn_3GaC - Mn_3GaN$ are grouped in Table III.6.

Table III. 6: Bulk modulus B, shear modulus (G_V, G_R and G_H), Young's modulus E, Poisson's ratio σ , and B/G ratio.

Compound	$B(GPa)$	$G_V(GPa)$	$G_R(GPa)$	$G_H(GPa)$	$E(GPa)$	σ	G/B
$\mathbf{Mn_3ZnC}$	387.80	241.52	230.14	235.83	439.95	0.584	0.60
$\mathbf{Mn_3GaC}$	422.60	271.25	260.66	265.95	489.69	0.586	0.63
$\mathbf{Mn_3GaN}$	360.25	213.88	207.48	205.6	398.80	0.581	0.57

Pugh's ratio is defined as the ratio of shear modulus to bulk modulus k = G/B, is generally used for the prediction of the ductility of materials.

The Pugh's ratio (k) and the Poisson's ratio (ν) are used to determine the brittle and ductile nature of the materials.

For Pugh's ratio, the boundary value is 0.571. If k<0.571, the compound is ductile otherwise, it is brittle. Our obtained values of k is: 0.60, 0.63, 0.57 for $Mn_3ZnC - Mn_3GaC - Mn_3GaN$ respectively. These values indicate that our compounds will behave as a brittle material because it is bigger than the critical value separating ductility and brittleness [23]. Also, Cauchy pressure ($P = C_{12} - C_{44}$) defined as the difference between the two elastic constants $C_{12} - C_{44}$ is considered as an indication of ductility. The positive value of P presents ductile nature, and its negative value characterises a material as brittle. The positive value of the Cauchy pressure indicates that Mn_3GaN is a ductile material and Mn_3ZnC, Mn_3GaC are brittle.

III.3.2.2 Elastic anisotropy

Elastic anisotropy shows the dependence of the mechanical properties of a material on the different crystallographic directions of the materials.

The formulas necessary to calculate elastic anisotropy for cubic structure are [24]:

$$\frac{1}{B} = \beta = S_{11} + 2S_{12} \quad \text{(III-9)}$$

$$\frac{1}{E} = S_{11} - 2\left(S_{11} - S_{12} - \frac{1}{2}S_{44}\right)(l_1^2 l_2^2 + l_2^2 l_3^2 + l_3^2 l_1^2) \quad \text{(III-10)}$$

For the cubic phase, the anisotropy factor given by the following relation:

$$A = \frac{2C_{44}}{C_{11} - C_{12}} \quad \text{(III-11)}$$

$$\text{si} \begin{cases} A = 1 \rightarrow \text{The material is isotropic} \\ A \neq 1 \rightarrow \text{The material is anisotropic} \end{cases}$$

For the anisotropy parameter, the values are equal to 0.63, 0.66, 0.70 for ($Mn_3ZnC - Mn_3GaC - Mn_3GaN$) respectively, which is not equal to unity and hence will present anisotropic nature.

The results of the Young's modulus calculation from equations (III-9, III-10) for the three compounds are presented in figures (III.14).

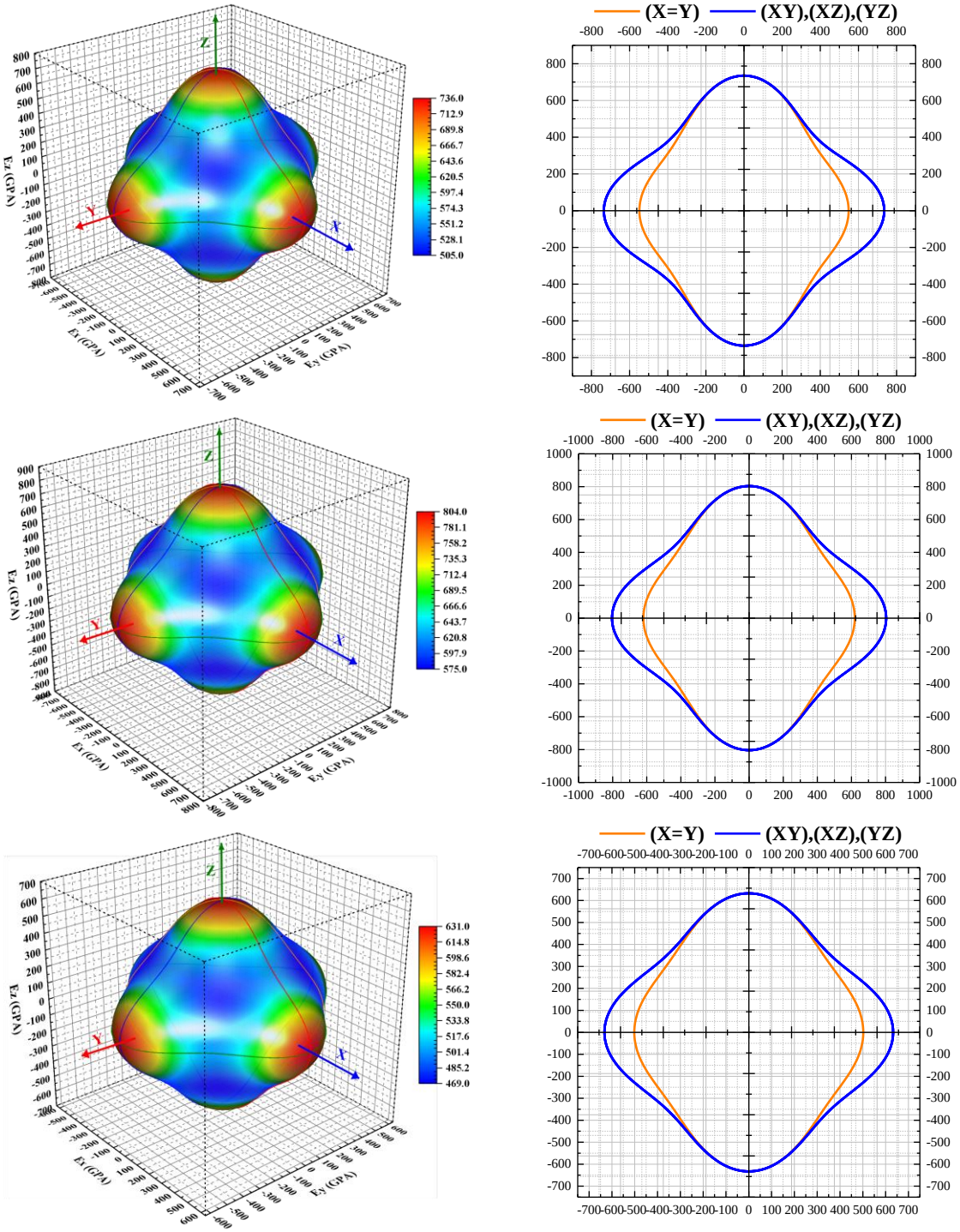

Figure III. 14: Young's modulus E in three and two dimensions for Mn_3ZnC-Mn_3GaC-Mn_3GaN respectively.

III.3.2.3 Isotropic elastic wave velocities and Debye temperature

According to the elastic constants obtained, we can compute the Debye temperature (θ_D), which is an important parameter related to many physical properties such as specific heat and melting temperature and reflects the stability of materials and the bond strength. The θ_D calculated by using average sound velocity ν_m by the following equations:

$$\theta_D = \frac{h}{k_B}\left[\frac{3n}{4\pi}\left(\frac{N_A\rho}{M}\right)\right]^{\frac{1}{3}}\nu_m \quad \text{(III-12)}$$

With ν_m is the mean sound speeds calculated by the following relationship:

$$\nu_m = \left[\frac{1}{3}\left(\frac{2}{\nu_t^3}+\frac{1}{\nu_l^3}\right)\right]^{-\frac{1}{3}} \quad \text{(III-13)}$$

where ν_t and ν_l are the transverse and longitudinal sound speeds, given by the following formulas:

$$\nu_t = \left(\frac{3B+4G}{3\rho}\right)^{\frac{1}{2}}, \quad \nu_l = \left(\frac{G}{\rho}\right)^{\frac{1}{2}} \quad \text{(III-14)}$$

Here, h is Planck's constant, k_B is Boltzmann's constant, N_A is Avogadro's number, ρ is the mass density, n is the number of atoms in the cell and M is the weight of unit cell.

Our computed values of Debye temperature (θ_D) are listed in Table III.7 These values of θ_D is large than that obtained in other works and comparable to experimental values.

Table III. 7: Calculated values of density ρ(g/cm3), wave speeds, and (m/s) and Debye temperature (θ_D) for the three compounds.

Compound		$\rho\ (g/cm^3)$	$v_l\ (m/s)$	$v_t(m/s)$	$v_m(m/s)$	$\theta_D(K)$
Mn_3ZnC	Our work	6.91	10081	5841,98	6483,58	855,51
	Other work[12]	-	6067	3197	4233	557
Mn_3GaC	Our work	4.14	13701,44	8014,93	8887,67	983,18
	Other work[25]	-	-	-	-	570.2
Mn_3GaN	Our work	7.63	9166,08	5253,71	5836,31	797,08
	Other work[26]	-	-	-	-	452.2

Decrease values as follows (Mn_3GaC>Mn_3ZnC>Mn_3GaN). In addition, a high Debye temperature indicates a high thermal conductivity, hence Mn_3GaC can be predicted to conduct heat better than both of Mn_3ZnC and Mn_3GaN.

Chapter III: Results and discussion

III.4. References

[1] Blaha, Peter, et al. "Full-potential, linearized augmented plane wave programs for crystalline systems." *Computer physics communications* 59.2 (1990): 399-415.

[2] Schwarz, Karlheinz, and Peter Blaha. "Solid state calculations using WIEN2k." *Computational Materials Science* 28.2 (2003): 259-273.

[3] Wu, Zhigang, and Ronald E. Cohen. "More accurate generalized gradient approximation for solids." *Physical Review B* 73.23 (2006): 235116.

[4] Dudarev, S. L., et al. "Electron-energy-loss spectra and the structural stability of nickel oxide: An LSDA+ U study." *Physical Review B* 57.3 (1998): 1505

[5] Albers, R. C., Niels Egede Christensen, and Axel Svane. "Hubbard-U band-structure methods." *Journal of Physics: Condensed Matter* 21.34 (2009): 343201.

[6] Benmalem, Y., et al. "Thermoelectric, electronic and structural properties of $CuNMn_3$ cubic antiperovskite." *Journal of Computational Electronics* 17.3 (2018): 881-887.

[7] Wen, Yongchun, et al. "Lattice, magnetic and electronic transport behaviors of Ge-doped Mn_3XC (X= Al, Zn, Ga)." *Journal of alloys and compounds* 489.1 (2010): 289-292.

[8] Fruchart, D., et al. "Structure magnetique de Mn_3GaC." *Solid State Communications* 8.2 (1970): 91-99.

[9] Bertaut, E. F., et al. "Diffraction neutronique de Mn_3GaN." Solid State Communications 6.5 (1968): 251-256.

[10] Wedepohl, P. T. "Comparison of a simple two-parameter equation of state with the Murnaghan equation." *Solid State Communications* 10.10 (1972): 947-951.

[11] Hoat, D. M. "Investigation on structural, electronic, magnetic and thermodynamic properties of antiperovskites Mn_3XC (X= Al, Zn and Ga)." International Journal of Modern Physics B 33.28 (2019): 1950337.

[12] Bouhemadou, A., et al. "Ab initio study of some fundamental physical properties of the cubic inverse-perovskite Mn_3ZnC and Mn_3GeC." Computational materials science 58 (2012): 162-166.

[13] Medkour, Y., et al. "Structural, elastic, electronic and magnetic properties of Mn_3ZnC and Mn_3GeC." Computational and Theoretical Chemistry 991 (2012): 161-164.

[14] Monkhorst, Hendrik J., and James D. Pack. "Special points for Brillouin-zone integrations." *Physical review B* 13.12 (1976): 5188.

[15] DJERMOUNI, Mostefa. "Electronic Structure and Magnetic Properties in Perovskite-Related Materials." PhD diss., 2015.

[16] Haddadi, Khelifa. "Etude des propriétés structurales, élastiques et électroniques des composés antiperovskites de type $XNCa_3$." PhD diss., Université de Sétif 1-Ferhat Abbas, 2013.

[17] Gonze, Xavier, et al. "First-principles computation of material properties: the ABINIT software project." *Computational Materials Science* 25.3 (2002): 478-492.

[18] Head, John D., and Michael C. Zerner. "A Broyden—Fletcher—Goldfarb—Shanno optimization procedure for molecular geometries." *Chemical physics letters* 122.3 (1985): 264-270.

[19] Born, M. and K. Huang, Dynamical Theory of Crystal Lattices, édité par Clarendon, 1956, Oxford.

[20] W. Voigt, Lehrbuch der Kristallphysik, Teubner-Verlag, Leipzig, 1928.

[21] A. Reuss, Berechnung der Fließgrenze von Mischkristallen auf Grund der Plastizitätsbedingung für Einkristalle, ZAMM 9(1) (1929), pp. 49–58.

[22] R. Hill, The elastic behaviour of a crystalline aggregate, Proc. Phys. Soc. A 65(5) (1952), pp. 349–3.

[23] S. Pugh, XCII. Relations between the elastic moduli and the plastic properties of polycrystalline pure metals, Lond. Edinb. Dublin Philos. Mag. J. Sci. 45(367) (1954), pp. 823–843.

[24] J._F._Nye, *Physical_Properties_of_Crystals_Their* CLARENDON PRESS · OXFORD.

[25] Baigutlin, D. R., et al. "Ab initio Calculation of vacancy formation energy in antiperovskite Mn3GaC." *Вестник Южно-Уральского государственного университета. Серия: Математика. Механика. Физика* 11.2 (2019).

[26] J. Zemen, E. Mendive-Tapia, Z. Gercsi, R. Banerjee, J. Staunton, and K. Sandeman, Frustrated magnetism and caloric effects in Mn-based antiperovskite nitrides: Ab initio theory, Phys. Rev. B 95(18) (2017), p. 184438.

“Never give up on a dream just because of the time it will take to accomplish it. The time will pass anyway.”

-Earl Nightingale

General Conclusion

General Conclusion

In summary, the theoretical calculations based on FP-LAPW method has been carried out to investigate the structural, electronic, magnetic properties of Mn_3AX (A: Zn and Ga), (X: C and N) antiperovskites. Considered ternaries are energetically stable in ferromagnetic state due to their lowest energy as compared with those of NM and AFM phases, which are confirmed with experimental reports. Calculated lattice constants are in good agreement with other available theoretical results, though they are slightly smaller than the experimental values. Electronic properties confirm the metallic behaviour of our three antiperovskites compounds and magnetic moment of them are generated mainly from the spin-polarization of Mn-3d orbital. In addition, our study has shown that using GGA approximation slightly underestimates the magnetic moments compared to the GGA+U, which has given us the known magnetic moments, then at the end, the effect of Hubbard potential was cancelled by the spin orbit coupling calculation and returned to the initial values.

Mn-C chemical bonding is mainly covalent resulting from the hybridization between Mn-3d and C-2p states, while Mn-X bonding has metallic nature as attraction between free electrons of Mn atom and positively charged X atoms.

The magnetic moment for these three compounds (Mn^{3+}) decreases under an applied pressure, which confirms an important magnetic reactivity of them that makes it an excellent candidate for magneto-mechanical applications.

The mechanical properties of these compounds have been investigated also, we have found that these compounds are stable mechanically and showed anisotropic character. The calculated results of Poisson's ratio, Pugh's ratio and Cauchy pressure show that the Mn_3GaN is ductile material and Mn_3ZnC, Mn_3GaC are brittle.

Abstract

The purpose of this work is the determination of the structural, electronic, magnetic, and mechanical properties of Mn-based antiperovskites Mn_3AX (A = Zn, Ga), (X=C, N). The calculations were performed in the framework of the density functional theory (DFT), within the two methods: pseudo potentials (PP) and the Full Potential Linear Augmented Planes Waves (FP-LAPW). The generalized gradient approximation proposed by Wu-Cohen (GGA-WC) is used for modeling exchange-correlation effects. The electronic structures and magnetic properties of Mn-based antiperovskites were studied using the GGA, GGA + U and spin orbit coupling methods. The inclusion of Hubbard U potential gives significant effects on the electronic density of states, the structure of the energy band and the magnetic moment. The results obtained were commented and compared with the available experimental data. A very good agreement was found between the calculated results and those obtained from the experimental. The mechanical properties of these compounds have been investigated also, and we have found that these compounds are stable mechanically and showed anisotropic character.

Key words: Density Functional Theory, antiperovskites structure, electronic structure, phase transition, structural stability, magnetic structure.

Résumé

Le but de ce travail est la détermination des propriétés structurales, électroniques, magnétiques et mécaniques des antipérovskites à base de Mn Mn3AX (A = Zn, Ga), (X=C, N). Les calculs ont été effectués dans le cadre de la théorie de la fonctionnelle de la densité (DFT), au sein des deux méthodes : les pseudo potentiels (PP) et les Full Potential Linear Augmented Planes Waves (FP-LAPW). L'approximation du gradient généralisé proposée par Wu-Cohen (GGA-WC) est utilisée pour modéliser les effets d'échange-corrélation. Les structures électroniques et les propriétés magnétiques des antipérovskites à base de Mn ont été étudiées en utilisant les méthodes de couplage GGA, GGA + U et spin orbite. L'inclusion du potentiel Hubbard U donne des effets significatifs sur la densité d'états électroniques, la structure de la bande d'énergie et le moment magnétique. Les résultats obtenus ont été commentés et comparés aux données expérimentales disponibles. Un très bon accord a été trouvé entre les résultats calculés et ceux obtenus à partir de l'expérimentation. Les propriétés mécaniques de ces composés ont également été étudiées et nous avons trouvé que ces composés sont stables mécaniquement et présentent un caractère anisotrope.

Mots clés: Théorie fonctionnelle de la densité, structure des antipérovskites, structure électronique, transition de phase, stabilité structurelle, structure magnétique.

ملخص

الغرض من هذا العمل هو تحديد الخصائص البنيوية والإلكترونية والمغناطيسية والميكانيكية لمضادات البيروفسكيت القائمة على المنغنيز .Mn Mn3AX (A = Zn, Ga), (X = C, N) وقد أجريت الحسابات في إطار النظرية الوظيفية للكثافة ، بإستعمال طريقتي الحساب: :(كل الالكترونات وأشباه الكمونات). ويستخدم التقريب المعمم للتدرج الذي اقترحه وو كوهين (GGA-WC) لنمذجة تأثيرات الترابط بين التبادل. ودُرست الهياكل الإلكترونية والخواص المغناطيسية لمضادات البيروفسكيت القائمة على المنغنيز باستخدام طرق التقارب GGA و GGA + U وطرق التقارب في المدار الدوراني. إن إدراج إمكانية هابارد يو يعطي تأثيرات كبيرة على الكثافة الإلكترونية للدول ، وهيكل نطاق الطاقة ، واللحظة المغناطيسية. وتم التعليق على النتائج التي تم الحصول عليها ومقارنتها بالبيانات التجريبية المتاحة. وتم التوصل إلى اتفاق جيد للغاية بين النتائج المحسوبة وتلك التي تم الحصول عليها من التجربة. وقد تم أيضا فحص الخصائص الميكانيكية لهذه المركبات ، ووجدنا أن هذه المركبات مستقرة ميكانيكيا و أظهرت طابع متباين الخواص.

الكلمات المفتاحية: نظرية الكثافة الوظيفية ، بنية مضادات البيروفسكيت ، البنية الإلكترونية ، المرحلة الانتقالية ، الاستقرار البنيوي ، البنية المغناطيسية.